

Manuscript Details

Manuscript number	JNM_2019_304_R1
Title	Nanoscale analysis of ion irradiated ODS 14YWT ferritic alloy
Article type	Full Length Article

Abstract

In this work, the nanoscale microstructure of an advanced oxide dispersion strengthened (ODS) 14YWT ferritic alloy (SM13 heat) with nominal composition Fe-14Cr-3W-0.4Ti-0.3Y₂O₃ (wt. %) has been characterized by atom probe tomography (APT) before and after ion irradiation with 70 MeV Fe⁹⁺ ions at 450oC to a total dose of 21 dpa. A detailed solute cluster analysis of APT data reveals that, in the manufacturing process, larger nanoparticles form in or close to the grain boundaries respective to those inside grains. The evolution of the nanoparticles after irradiation seems to be related to their location, as a higher increase in the number density and in the Y:Ti ratio is observed for the nanoparticles in or close to grain boundaries. APT analysis also shows Cr, W and C segregation to grain boundaries enhanced by the irradiation. A previous study of this same alloy before and after irradiation reports that the mechanical properties do not seem to be affected, but the microstructure was not investigated to confirm. The present work confirms little microstructural evolution after irradiation in this 14YWT alloy, indicating tolerance at the given irradiation conditions.

Manuscript category	Structural materials
Corresponding Author	Maria A Auger
Corresponding Author's Institution	Universidad Carlos III de Madrid
Order of Authors	Maria A Auger, David Hoelzer, Kevin Field, Michael Moody
Suggested reviewers	Jan Hoffmann, Kristina Lindgren, Mukesh Bachhav

Submission Files Included in this PDF

File Name [File Type]

Cover letter.docx [Cover Letter]

JNM_2019_304_R1_Response to reviewers.pdf [Response to Reviewers]

JNM_2019_304_R1_Manuscript with tracked changes.docx [Revised Manuscript with Changes Marked]

JNM_2019_304_R1_Manuscript_without_tracked_changes.docx [Manuscript File]

Fig1.tif [Figure]

Fig2.tif [Figure]

Fig3.tif [Figure]

Fig4.tif [Figure]

Fig5.tif [Figure]

Fig6.tif [Figure]

Fig7.tif [Figure]

Fig8.tif [Figure]

Fig9.tif [Figure]

Fig10.tif [Figure]

Fig11.tif [Figure]

Table I.docx [Table]

Table II.docx [Table]

Table III.docx [Table]

Table IV.docx [Table]

Conflict_of_Interest_statement.pdf [Conflict of Interest]

To view all the submission files, including those not included in the PDF, click on the manuscript title on your EVISE Homepage, then click 'Download zip file'.

Research Data Related to this Submission

There are no linked research data sets for this submission. The following reason is given:
Data will be made available on request

Dear Editor,

We are submitting the results of our recent work in which we have characterized an oxide dispersion strengthened (ODS) 14YWT alloy (SM13 heat), as-received and after heavy ion irradiation with 70 MeV Fe ions at 450°C to a total dose of 21 dpa. After performing an atom probe tomography nanoscale analysis we found little microstructural changes after irradiation. Our results support those recently published by A. Prasitthipayong et al. (<https://doi.org/10.1016/j.nme.2018.05.018>), who performed a micro mechanical characterization study on this same alloy and found similar hardness and modulus values for the material before and after the mentioned heavy ion irradiation. Therefore, radiation stability of the 14YWT (SM13 heat) alloy can be confirmed, at least at the given irradiation conditions.

In my own name, and on behalf of my co-authors, we would be pleased if our work could be considered for publication in Journal of Nuclear Materials.

Yours sincerely,

Maria A Auger

Maria A Auger, PhD

Senior Research Fellow

Physics Department - Universidad Carlos III de Madrid

Avenida Universidad 30

28911 Leganés, Madrid (Spain)

Tel. +34 91 6249478

Email. mauger@fis.uc3m.es

Dear Professor Was,

We thank both you and the reviewers for your feedback. We list the reviewers' comments below and reply point-by-point to all of them. The manuscript has been revised and amended accordingly and all changes have been highlighted in the text.

Reviewer #1:

This study has the potential to add meaningful data to the larger collection of information capturing the irradiation evolution of oxide nanoclusters in ODS alloys. One distinct advantage of this study is the apparent high quantity of datasets available, enabling a larger analysis region for characterization. However, I am struggling mightily with gaining confidence in the data presented in this manuscript. As a result, it is difficult to reach the same conclusions as the authors.

First, it would be helpful for the authors to provide much more information about the methodology used for the APT analysis. This not only adds confidence for the reader, but also makes it easier to potentially compare the results of this study to that of another study. In particular, more detail about the methodology of dataset reconstruction in IVAS is needed. What was the procedure for identifying the image compression factor (ICF) or the k-factor for reconstruction? Was reconstruction done in voltage mode, shank mode, or using the tip profile? Figures 2A, and 8B appear to be severely distorted (e.g. "stretched" in the horizontal direction), which is usually an effect of selecting an inappropriate ICF value for reconstruction.

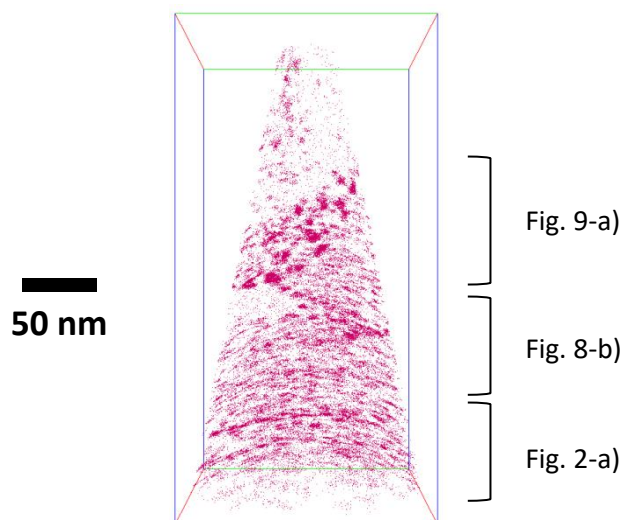
There was insufficient quality crystallographic information to utilise the identification of poles to calibrate the ICF. Instead, all APT reconstructions were calibrated by setting shank angle + tip radius values based on SEM images of the FIB prepared samples. The following text has been added in the Materials and Methods section (page 5, line 14):

'The analyzed volumes were reconstructed by setting shank angles and tip radii values from SEM images of the FIB prepared samples'

As mentioned in the Results section (page 6, line 5):

'As the size of the oxygen-enriched clusters within the grains may be different from those in or close to grain boundaries, they were analyzed separately by splitting the datasets into customized regions of interest (ROI) containing the relevant volumes.'

Figure 2-a) is actually one region of interest (ROI) from a larger dataset as described in the figure below:



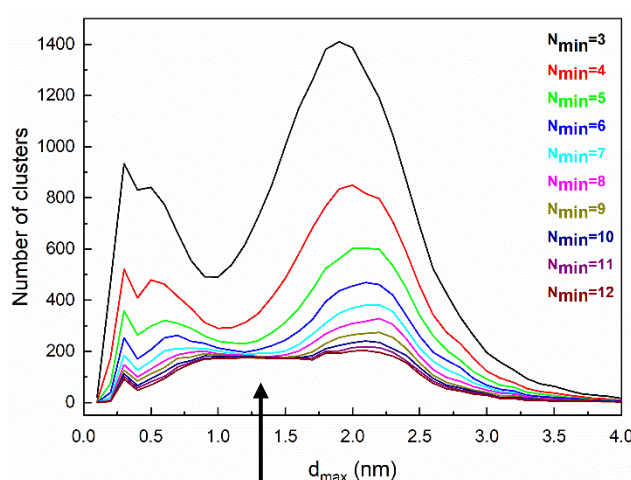
Localized regions of the nanostructure, e.g. grain boundaries and precipitates, can require significantly different levels of electric field intensity to be evaporated in the experiment compared to the surrounding iron matrix. This leads to the formation of highly localized regions of different curvature on the specimen throughout the analysis, violating the reconstruction assumption that the evaporation field is constant and that the tip is a perfect hemisphere. This results in the distortions to which Reviewer #1 refers. These aberrations cannot be rectified using standard reconstruction calibration methods. This same effect can be observed in the literature, for example in the figures from A. Certain et al. work (<https://doi.org/10.1016/j.jnucmat.2012.11.021>)

Next, I recommend providing much more detailed description about how the maximum separation method was implemented. Most notable, how was d_{max} and N_{min} determined for each dataset? I also recommend moving this detailed description into the "Materials and Methods" section of the manuscript, instead of the results section as it is currently placed.

Description of the maximum separation method has been moved to the "Materials and Methods" section (page 5, line 16) as:

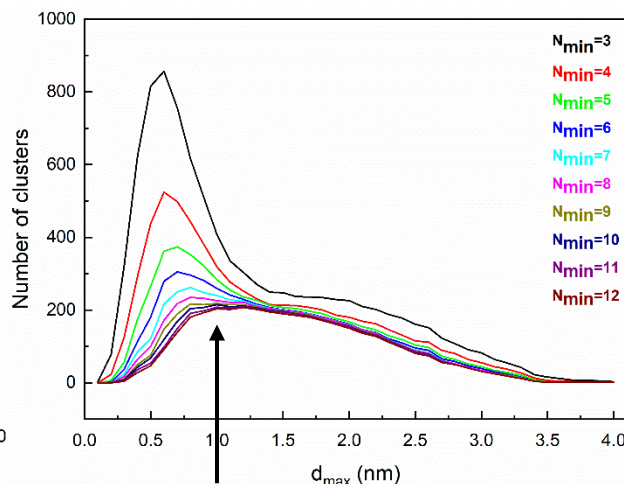
'The cluster analysis was made by implementing the maximum separation method [21]; this method defines clusters by setting a minimum number of ions, N_{min} , separated from each other a distance shorter than d_{max} . The cluster selection parameters, N_{min} and d_{max} , for each dataset were defined according to the criteria developed in [22]. The cluster size was calculated as the Guinier diameter, i.e. twice the Guinier radius [23]; and the distance between clusters was taken as the average distance between the center of mass [24] of one cluster and the center of mass of its first neighbor.'

To select appropriate values of the parameters defining the maximum separation algorithm, criteria developed in reference [22] (C. Williams et al. <https://doi.org/10.1016/j.ultramic.2012.12.011>) plot the Number of Clusters counts vs. d_{max} over a range of N_{min} values. By visual inspection the optimal d_{max} value can be defined as those values where the Number of Clusters across the different values of N_{min} converges to a single value (or at least close to a single value). We have applied these criteria to all the datasets in our work; we display below its application to 2 of the datasets displayed:



$N_{min} = 8, d_{max} = 1.3 \text{ nm}$

Dataset displayed in Fig. 2-b)



$N_{min} = 9, d_{max} = 1.0 \text{ nm}$

Dataset displayed in Fig. 10-a)

The visual appearance of the oxide nanoclusters in the Figures does not seem to match the data provided in Table II. In particular:

a) The average size of nanoclusters ranges 1.64-2.29 nm in diameter. If the average size of clusters is ~ 2 nm in each specimen, the clusters would visually appear to be only the size of 1/20th of the scalebar in Fig. 2, 3b, 8b, 9, and 11a-c, rendering them to be very small. However, by visual inspection of these Figures, there are clearly much larger clusters present, while clusters of the size tabulated are possibly invisible. My speculation is that the cluster analysis is spuriously detecting smaller oxide clusters that may not actually exist.

The numerical values included in Table II should be interpreted in context with the complementary histogram analyses displayed in Fig. 4, which, apart from the dispersion up to 9 nm, support the measured average size of the clusters. Statistics in Table II summarize analysis of 3097 clusters, so visual analysis in this case may be misleading.

If we recall the graph displayed in this document above (from the dataset displayed in Fig. 2-b)), the plot of Number of Clusters vs. d_{\max} for $N_{\min} = 3$ is instructive as it exhibits two maxima: the left maximum means that the choice of those clustering parameters is splitting ions from one larger cluster into artificially smaller clusters. The right maximum refers to clustering parameters that are artificially merging adjacent clusters into a single erroneously defined cluster. Thus, this acts as a guide in our choice cluster selection parameters: by selecting parameters in between those values, we have confidence that we are avoiding the selection of artificially small or artificially large clusters. Note that, if the Number of Clusters vs. d_{\max} plots do not exhibit two maxima we cannot make this assumption, however, the d_{\max} values we have used are in the range of 0.7 – 1.3 nm for all the datasets and, from all of our analyses we believe this to be large enough to avoid spuriously detecting small clusters not physically present in the analyzed volume.

b) The number densities provided in Table II also seem high compared to the visual Figures. Number densities of this magnitude are typically found in specimens experiencing alpha-prime separation of Cr from Fe when high Cr content is present. From personal experience and inspection of the figures, the densities should be at least one order of magnitude lower, once again that spurious detection of smaller clusters may be present.

We again highlight that visual inspection of statistics summarizing a large number of clusters (a total of 3097 split in 1104, 327, 742 and 924 subsets) may be misleading. Number densities of clusters in ODS alloys are frequently found in the literature as 10^{23} - 10^{24} m⁻³ range. This can be seen in the following works by:

Pasebani et al. (<https://doi.org/10.1016/j.jnucmat.2015.03.040>)

Rogozhkin et al. (<https://doi.org/10.1016/j.jnucmat.2010.09.021>)

He et al. (<https://doi.org/10.1016/j.jnucmat.2014.03.024>)

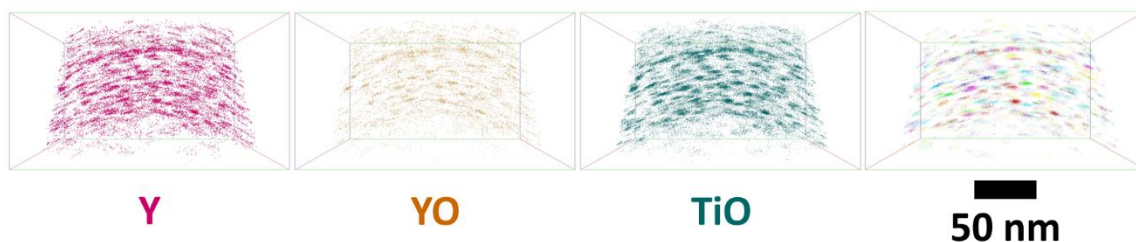
reporting number densities in the order of 10^{24} m⁻³ for clusters in ODS alloys.

We have not observed alpha-prime separation of Cr from Fe in any of the samples analyzed, so we cannot correlate our numeric results to that case.

A way to increase confidence in the data and prove that you have not spuriously identified clusters is to provide more visual evidence in the Figures. For example, you may use isoconcentration surfaces to identify clusters based on a concentration threshold and show these images. Furthermore, you could add images to your Figures showing the colored cluster maps from IVAS, with each identified cluster appearing in a different color. Then, if you put the reconstruction image, the isoconcentration image, and the cluster identification image side-by-side, you should see consistency between all three, increasing your confidence in the cluster identification. Without this information available to the reader, it is difficult to determine if you identified clusters correctly or not.

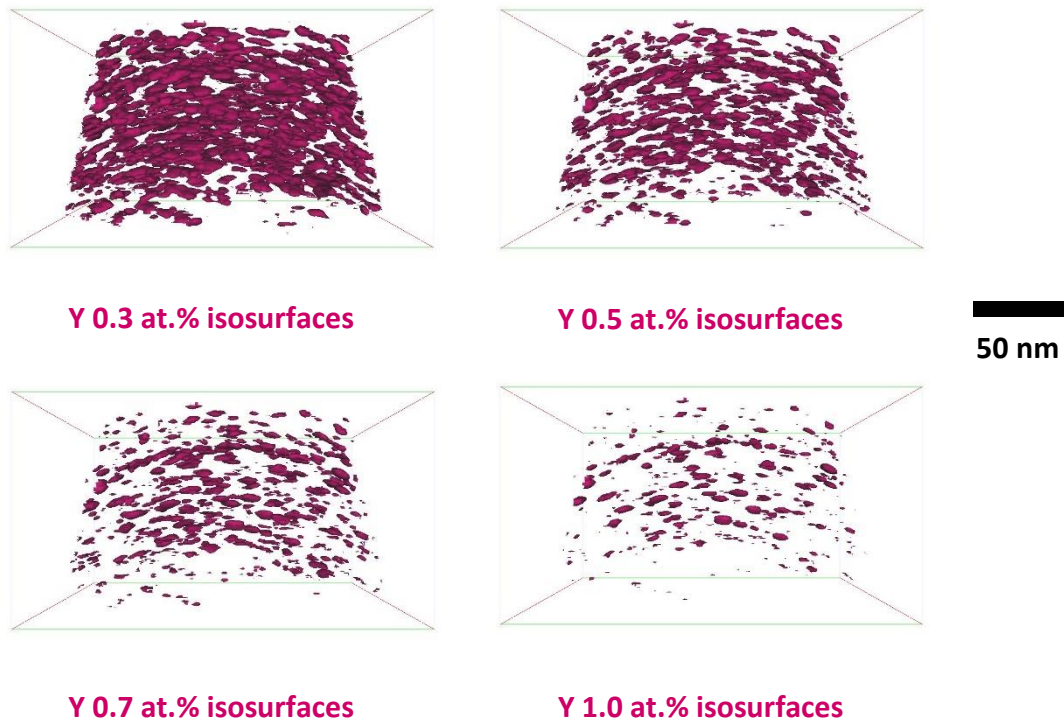
Based on this, my recommendation is to do a much more thorough job with the cluster analysis and share more details with the readers so that there is no question about the validity of the data.

We are now including the indexed and colored cluster maps in all the images. New Fig. 2-a) is displayed below as an example.



The isoconcentration surface selection is not applicable in our case, we show an example below for Fig. 2-a). The colored cluster map seems to highlight the clusters visually identified in the ion maps, while none of the isoconcentration surfaces, generated for different values of Y-concentration, appear to agree. We cannot take the isoconcentration approach as reliable because we observe many instances of:

- 'necking' joining adjacent clusters, leading to incorrect cluster size measurements
- complete failure to detect smaller clusters which are definitively identified by the maximum separation method,
- 'open surfaces' that cannot be taken as a cluster, which is defined as a bounded surface.



Some other key observations and questions:

In the "Materials and Methods" section, you identify that you used three dual beam FIB/SEM instruments, yet only two are listed. Furthermore, can you provide the motivation for using two/three different instruments.

In page 5, lines 4 – 7, we say ‘Needle-shaped samples for atom probe characterization were prepared by the lift-out method [20] using three dual beam FIB/SEM instruments: a FEI Helios NanoLab 600i at the Materials Research Facility (MRF) in Culham Center for Fusion Energy (CCFE), and a Zeiss Auriga 40 and a Zeiss NVision 40 at the Department of Materials, University of Oxford.’

This paragraph denotes the use of 3 instruments indeed:

1-FEI Helios Nanolab 600i at CCFE

2-Zeiss Auriga 40 at Oxford Materials

3-Zeiss NVision 40 at Oxford Materials

There was no specific motivation to use 3 FIB microscopes but a necessity to do it. The non-irradiated samples were received from the project partners a few months after we started analyzing the irradiated ones. FIB instruments operating times are often interrupted by vacuum, electron beam, ion beam, gas supply, micromanipulator and/or software problems. Over the time we were working on these samples we had to prepare APT samples and sort out the FIB time and access by using these 3 instruments; the institutions hosting them do ask for that use being acknowledged.

We believe that the choice of FIB/SEM has no influence on the presented results and hence the explanation above is superfluous to the paper.

Similarly, for the LEAP analysis, it appears two different instruments were used. It would be helpful to understand the motivation for this, and it is crucial to identify any fundamental differences with these instruments and how they may impact the integrity of the data. For example, do the two LEAP instruments have different detector efficiencies? If so, it is important to acknowledge this.

The use of two LEAP instruments is related to the point explained in the previous comment about receiving the irradiated and non-irradiated samples at such different times combined with atom probe instrument availability. In Oxford, we have access to two APT instruments: a LEAP 3000HR and a LEAP 5000XR. In page 5, lines 12 – 13, in the manuscript it is stated:

‘A total of 15 high quality datasets, containing between 1 and 30 million ions, were analyzed.’

Only 2 datasets (results shown in Figs. 3-b and 11-a Additional data) were obtained using a LEAP 3000HR whereas the other 13 were generated by the LEAP 5000 XR. The Reviewer is correct to highlight the difference in detection efficiency between the two instruments: 37% for the LEAP 3000 and 52% for the LEAP 5000. At Oxford we have previously undertaken a robust study of the effect of these differences: T.L. Martin et al. (*Comparing the Consistency of Atom Probe Tomography Measurements of Small-Scale Segregation and Clustering Between the LEAP 3000 and LEAP 5000 Instruments* <https://doi.org/10.1017/S1431927617000356>). We specifically demonstrate that the reliability of APT analysis of clusters in ODS steels is consistent between the two exact instruments used in the current work. That study suggests to customize the cluster analysis parameters to data obtained from each instrument, and we have rigorously applied this to each individual dataset.

It would be helpful to provide some dimensional context of the size of the bulk specimens in Fig. 1.

Scale bars have been included in Fig. 1.

In Table I, please clarify what the +/- symbols represent. I assume this is because you took 15 measurements within each of your datasets. Consider combining all of your datasets into a total analysis volume and then calculate the overall compositions instead.

The numerical values in Table I are actually the overall composition results of combining all the datasets (8 from the as-received sample and 7 from the ion irradiated sample) into a total analysis volume in each case. The statement:

'The resulting bulk composition is provided in Table I together with the composition obtained from APT analysis.'

has been replaced by:

'Table I summarizes the resulting bulk composition analysis performed by ORNL together with the average bulk and matrix compositions obtained from APT analysis (8 datasets for the as-received 14YWT sample and 7 datasets for the ion irradiated sample).'

in the Materials and Methods section (page 4, lines 14 – 16).

In Table II, it would be helpful to understand how you calculated the volumetric density of the clusters on the grain boundaries. Typically, grain boundaries are ~2D features, so you must have made some assumption or accommodation to measure volumetric density.

In the Results section (page 6, lines 5 – 7) we state that:

'the size of the oxygen-enriched clusters within the grains may be different from those in or close to grain boundaries'

When we discuss clusters at grain boundaries we actually refer to the clusters found in the grain boundaries, considered as the 2D features pointed out by the reviewer, and in their proximity regions.

We have substituted the phrase '*Clusters at grain boundaries*' by '*Clusters in, or close to, grain boundaries*' everywhere in the manuscript in order to avoid misunderstanding:

In Table IV, how may grain boundaries were analyzed to generate this data?

5 interfaces were analyzed in the as-received sample and 10 in the irradiated one. An extra line has been added to Table IV including this information.

Finally, toward the end of the "Cluster Analysis" section, you state, "...the nanoparticle size after irradiation is very similar to the nanoparticle size in unirradiated state, contrary to Wharry et al. [9]...". Meanwhile, earlier you state that ref [9] reports "a large variation of results regarding the evolution of nanoparticles in ODS steels under irradiation". Your conclusion that your results demonstrating stable size are in contrast to ref. [9] is not accurate.

The reviewer is correct, we have removed the citation to Wharry et al. work here (page 8, line 22).

Reviewer 2

The aim of this work is unclear. I don't understand why this work is needed.

See response to editor below.

Editor's comment:

Please note that papers published in JNM must contain new knowledge that advances the field. It is not clear from this paper what that is. You will need to address this in your revision.

We have characterized an ODS alloy ion irradiated at a high dose (21dpa) and at a reactor relevant temperature of 450°C, and observed subtle changes in the microstructure of the alloy before and after irradiation. Hence this work provides critical new nanoscale insights into the microstructure stability of irradiated ODS Fe-Cr alloy, further confirming its irradiation resistance and keeping it as a promising candidate for use in Gen IV and fusion reactors. As mentioned by Reviewer #1, results from a high quantity of datasets enable characterization of a larger analysis region, which represents a distinct advantage of our study. We are also complementing the micro-mechanical characterization results published by our Project partners, Prasitthipayong et al. (<https://doi.org/10.1016/j.nme.2018.05.018>) by providing complementary microstructural characterization which supports their observations and our conclusion of irradiation resistance of the ODS alloy. These points are expressed in the manuscript (Abstract, Introduction and Conclusions), but we take the chance to highlight them here in our response.

Many thanks for the valuable comments and suggestions. We hope that our answers and the revised manuscript make it suitable for publication in Journal of Nuclear Materials.

Yours faithfully,

A handwritten signature in black ink, appearing to read 'M. A. Auger', with a stylized flourish at the end.

Maria A Auger (on behalf of all the authors)

Nanoscale analysis of ion irradiated ODS 14YWT ferritic alloy

Maria A. Auger^{1,2*}, David T. Hoelzer³, Kevin G. Field³, Michael P. Moody²

¹Physics Department, Universidad Carlos III de Madrid. Avenida Universidad 30, 28911

Leganés, Madrid, Spain.

²Department of Materials, University of Oxford. Parks Road OX1 3PH, Oxford, UK.

³Oak Ridge National Laboratory, Oak Ridge, TN 37831, Tennessee, USA.

*Corresponding Author: Tel. +34 91 624 9478, Fax. +34 91 624 8749, e-mail address:

mauger@fis.uc3m.es

Abstract

In this work, the nanoscale microstructure of an advanced oxide dispersion strengthened (ODS) 14YWT ferritic alloy (SM13 heat) with nominal composition Fe-14Cr-3W-0.4Ti-0.3Y₂O₃ (wt. %) has been characterized by atom probe tomography (APT) before and after ion irradiation with 70 MeV Fe⁹⁺ ions at 450°C to a total dose of 21 dpa. A detailed solute cluster analysis of APT data reveals that, in the manufacturing process, larger nanoparticles form **in or close to** the grain boundaries respective to those inside grains. The evolution of the nanoparticles after irradiation seems to be related to their location, as a higher increase in the number density and in the Y:Ti ratio is observed for the nanoparticles **in or close to** grain boundaries. APT analysis also shows Cr, W and C segregation to grain boundaries enhanced by the irradiation. A previous study of this same alloy before and after irradiation reports that the mechanical properties do not seem to be affected, but the microstructure was not investigated to confirm. The present work confirms little microstructural evolution after irradiation in this 14YWT alloy, indicating tolerance at the given irradiation conditions.

Keywords

14YWT, ODS alloys, atom probe tomography, ion irradiation, clusters

Introduction

Oxide dispersion strengthened (ODS) steels and ferritic alloys have remained candidate structural materials for nuclear applications in Gen IV reactors over the last decade due to the dispersion of nano-size oxide particles (nanoparticles) improving their mechanical performance and radiation tolerance [1–7]. The presence of nanoparticles plays an essential role in these behaviors by impeding dislocation motion and cavity growth, which in turn enhances the creep resistance while simultaneously reducing the impacts of irradiation. The nanoparticle dispersion thus allows for exposure to increased operating temperatures and radiation dose regimes compared to conventional ferritic alloys [8].

Results from a variety of experimental conditions, including different manufacturing routes, alloy compositions and irradiation parameters, have been recently summarized by J. Wharry et al. in [9] and, apart from experimental differences, the ODS alloys generally show resistance under irradiation for typical operating conditions of nuclear power reactors in terms of microstructural evolution and radiation-induced hardening. For instance, D.A. McClintock et al. [10] characterized 14YWT exposed to 1.5 dpa neutron irradiation at 300 – 750°C and found good resistance to radiation-induced hardening. This was attributed to the fine grain structure and high number density of nanoclusters in the alloy. A. Certain et al. [11] studied a 14YWT alloy (SM10 heat), similar to the alloy presented in this work, irradiated with protons (to 1 and 3 dpa at 400°C) and Ni²⁺ ions (to 50 and 100 dpa from - 75°C to 600°C). They observed dissolution of the nanoclusters after heavy-ion irradiation at

cryogenic temperatures, while little to no changes were observed in samples irradiated at reactor relevant conditions (600°C). M. Šćepanović et al. [12] submitted a 14YWTi alloy to triple ion (Fe^{5+} , He^+ and H^+) irradiation at 600°C and to single ion (Fe^{5+}) irradiation at -80°C, and confirmed the stability of the nanoparticles after both irradiation experiments, with only slight differences regarding the size and composition of the nanoparticles observed. However, as highlighted in [9], even though results from a large number of studies are available, there is a high difficulty in normalizing these observations across the wide range of irradiation sources, dose rates, temperatures and different compositions of irradiated ODS alloys that have been investigated. Hence, clear conclusions regarding the evolution of the nanoparticles under irradiation at common nuclear power reactor temperatures have yet to be established. A similar observation can be made regarding radiation induced segregation in high chromium Fe-based body-centered cubic alloys. The literature provides a wide range of studies [13–16], but a clear conclusion cannot be reached, as segregation and depletion of solute atom concentration to specific regions of the microstructure have been reported, along with other cases where no apparent change is observed. Therefore, further experimental and theoretical studies are needed in order to understand and predict the evolution of these alloys under irradiation.

The aim of this work is to contribute to that effort by characterizing the nanoscale microstructure of the advanced ODS 14YWT ferritic alloy (SM13 heat) with nominal composition Fe-14Cr-3W-0.4Ti-0.3Y₂O₃ (wt. %), before and after irradiation with a high energy (70 MeV) Fe^{9+} ion beam to 21 dpa at 450°C. The atom probe tomography (APT) characterization technique has been used to perform a detailed cluster analysis and radiation induced segregation (RIS) effects study.

Materials and Methods

The ODS 14YWT ferritic alloy (SM13 heat) was produced by mechanical alloying at Oak Ridge National Laboratory (ORNL) [17]. Gas atomized powder (Special Metals, Inc.) of composition Fe-14Cr-3W-0.4Ti (wt. %) was ball milled with 0.3 wt.% Y₂O₃ powder (Nanophase, Inc.) using a high kinetic energy CM08 Simoloyer (Zoz, GmbH) for 40 h in Ar atmosphere. The milled powder was canned in mild steel, degassed for 24 h at 300°C under vacuum and consolidated by hot extrusion through a rectangular-shaped die after a heat treatment of 1 h at 850°C. A plate was produced from the extruded bar by cross rolling at 1000°C, reaching a 50% reduction in thickness. The mild steel can was kept on the extruded ODS 14YWT bar during cross rolling to avoid additional contamination. Images of the sample at different stages can be seen in Fig. 1. The C and S bulk composition was measured by combustion infrared detection, the O and N was determined from inert gas fusion, while all other alloying elements bulk composition was determined using direct current plasma emission spectroscopy. The resulting bulk composition is provided in Table I together with the composition obtained from APT analysis. Table I summarizes the resulting bulk composition analysis performed by ORNL together with the average bulk and matrix compositions obtained from APT analysis (8 datasets for the as-received 14YWT sample and 7 datasets for the ion irradiated sample).

The irradiation experiment was held at the Center of Accelerator Mass Spectrometry (CAMS), Lawrence Livermore National Laboratory (LLNL), CA using a rastered beam of 70 MeV Fe⁹⁺ ions to a total accumulated dose of 21 dpa and dose rate of 3.7×10^{-4} dpa/s at a nominal temperature of 450°C (the original dose is 20.68, as quoted by A. Prasitthipayong et al. in [18]). The actual temperature, monitored by an IR camera and a thermocouple behind the sample, was 456 ± 11 °C averaged over the 15.55 h irradiation time. The average current

was 19.47 nC/s, measured using an array of micro Faraday cups. SRIM simulations [19], using a displacement energy of 40 eV and a ion flux value of 10^{15} ions/cm² in the modified Kinchin–Pease model of the SRIM-2013 software version were made. These calculations predict that the damage layer will extend approximately to a depth of 6.2 μm from the sample surface [18].

Needle-shaped samples for atom probe characterization were prepared by the lift-out method [20] using three dual beam FIB/SEM instruments: a FEI Helios NanoLab 600i at the Materials Research Facility (MRF) in Culham Center for Fusion Energy (CCFE), and a Zeiss Auriga 40 and a Zeiss NVision 40 at the Department of Materials, University of Oxford. The APT analysis was performed at the Department of Materials, University of Oxford. A CAMECA LEAP™ 3000X HR in laser mode ($\lambda = 532$ nm, 0.40 nJ laser energy) at a repetition rate of 200 kHz and a CAMECA LEAP™ 5000XR operating in laser mode ($\lambda = 355$ nm, 0.040 – 0.050 nJ laser energy) at a repetition rate of 200 kHz were used; the sample temperature was always kept at 50-55K. A total of 15 high quality datasets, containing between 1 and 30 million ions, were analyzed. CAMECA IVAS™ software together with Origin®, MATLAB® and Corel® Photo-Paint® were used to produce the results and figures in this work. The analyzed volumes were reconstructed by setting shank angles and tip radii values from SEM images of the FIB prepared samples. The cluster analysis was made by implementing the maximum separation method [21]; this method defines clusters by setting a minimum number of ions, N_{min} , separated from each other a distance shorter than d_{max} . The cluster selection parameters, N_{min} and d_{max} , for each dataset were defined according to the criteria developed in [22]. The cluster size was calculated as the Guinier diameter, i.e. twice the Guinier radius [23]; and the distance between clusters was taken as the average distance between the center of mass [24] of one cluster and the center of mass of its first neighbor.

Results

Reconstructed 3D maps showing the Y, Y-O and Ti-O ion distributions in the as-received and irradiated 14YWT alloy are shown in Figs. 2 and 3, respectively. C ion maps are also included to highlight the presence of grain boundaries, as C was found to segregate to grain boundaries in both the as-received and irradiated conditions. Ion map reconstructions from all the datasets used in this study are included as Supplementary material. As the size of the oxygen-enriched clusters within the grains may be different from those in or close to grain boundaries, they were analyzed separately by splitting the datasets into customized regions of interest (ROI) containing the relevant volumes.

The cluster analysis was made by implementing the maximum separation method [21]. The cluster size was calculated as the Guinier diameter, i.e. twice the Guinier radius [23]; and the distance between clusters was taken as the average distance between the center of mass [24] of one cluster and the center of mass of its first neighbor. The size distribution of clusters inside grains and in grain boundaries for as-received and irradiated 14YWT is shown in Fig. 4, and a summary of the cluster analysis statistics is included in Table II. In the as-received sample, clusters in or close to the grain boundaries are 27 % larger than those inside grains and, in the irradiated sample, this difference in size is 31 %. On the other hand, the average size of the clusters inside grains is very similar in the as received and irradiated states, respectively, of 14YWT, and a similar observation can be made when comparing the clusters in or close to grain boundaries.

A 40 % and 46 % increase in the average number density of nanoparticles after irradiation can be observed respectively inside grains and in or close to grain boundaries (Table II).

In addition, the cluster separation distance was found to be 4% and 3% closer in the irradiated state compared to the as-received sample, respectively inside grains and **in or close to** grain boundaries (Table II).

Regarding the cluster composition, the chemistry of all the analyzed clusters is graphically displayed in Fig. 5 and summarized in Table III. In this case, a variation in the Y and Ti content can be observed in the irradiated state compared to the as-received condition, with average Y content increasing and Ti content decreasing **both for clusters inside grains and in or close to grain boundaries**. It is worth noting that there is a large variation of stoichiometry in the analyzed clusters, especially in the smaller ones, as it has been observed in previous studies [11,12].

The Y:Ti ratio after irradiation increases in the clusters located inside grains and **in or close to** grain boundaries by 27% and 47%, respectively. The (Y+Ti):O ratio remains almost constant, in the 1.44 – 1.48 narrow range, for all the analyzed clusters.

An important radiation effect is the segregation of elements (Cr, W and C) to grain boundaries. Figs. 6 and 7, show 1D elemental concentration analysis across grain boundary interfaces for the as-received and irradiated samples, respectively. The peak compositions for each element are summarized in Table IV. Peak at. % concentration values for Cr and W are 27% and 9% higher after irradiation, respectively. C segregation is highly enhanced by the irradiation, with a peak value 8.4 times higher than in the as-received state. The size of the segregation interface is measured as the distance between minimum concentration values around the segregation peak. The interface width was observed to be 20% narrower in the irradiated state compared to the as-received sample (Table IV).

Discussion

Cluster analysis

Distinction of cluster behavior after irradiation by considering their location, inside grains and **in or close to** grain boundaries, is not usually considered in the literature. In our study, differences in the nanocluster evolution are apparent depending on their location in the microstructure. In the as-received alloy, nanoparticles **in or close to** grain boundaries are larger than those inside grains, but their size remains unchanged after irradiation at both locations. The number density of nanoclusters is lower **in or close to** grain boundaries than inside grains in the as-received state. After irradiation, this value increases in both locations and the clusters are found to be closer together.

As reported in [9], there is a large variation of results regarding the evolution of nanoparticles in ODS steels under irradiation, making it very difficult to establish a specific mechanism describing the effects of irradiation taking place. Actually, a combination of several mechanisms including ballistic dissolution, Ostwald ripening and irradiation-enhanced diffusion seem to justify the observed evolution of clusters in irradiated ODS steels.

By ballistic dissolution [25] atoms can be ejected from clusters as a consequence of the ballistic collisions from irradiation damage cascades. APT sample volumes typically contain clusters < 10 nm in size, but TEM studies usually report the presence of larger clusters in ODS alloys [26,27]; these larger clusters would be more likely to follow ballistic dissolution for being a bigger cross-sectional target. The ejected atoms can subsequently diffuse back into the initial cluster, diffuse to a different cluster or diffuse into the matrix. Those diffusing into the matrix can initiate homogeneous nucleation (inside grains) or heterogeneous nucleation (at grain boundaries or other defects), with this last one being more energetically favorable [28]. Nanoparticles that are nucleated from the ejected solutes will grow until

reaching a steady-state size determined by the balance in flux of solutes being ejected and attached. In our study, there is an increase of 46% in the number density of clusters **in or close to** grain boundaries compared to the 40% increase for clusters inside the grains. Also, the nanoparticle size after irradiation is very similar to the nanoparticle size in unirradiated state, **contrary to Wharry et al. [9], who concluded that the average cluster size was reduced due to irradiation.**

The Y:Ti ratio increases after irradiation, consistent with other studies in the literature [29–31], suggesting that Ti atoms are more easily displaced from nanoclusters than Y atoms and, in our specific case, Ti atoms are more prone to displace **in or close to** grain boundaries than inside grains.

The (Y + Ti):O ratio remains constant; this observation may confirm that the displacement of O atoms and ejection of Ti atoms take place at the same rate [31].

Dissolution, nucleation and coarsening mechanisms act simultaneously during irradiation and, according to the experimental results presented here, they seem to happen at different rates inside grains **and in or close to** grain boundaries.

Radiation-induced segregation

Radiation-induced segregation (RIS) is known to be a non-equilibrium process which produces point defects that, depending on the irradiation temperature, can be mobile and relocate to defect sinks like surfaces, grain boundaries or dislocations [32]. Components which diffuse more quickly via interstitials will tend to segregate to grain boundaries, while components which diffuse more quickly via vacancies will tend to deplete.

A specific trend regarding radiation-induced segregation of elements in irradiated ODS steels cannot be found in the literature, as both segregation, depletion or no change of elements to grain boundaries and dislocations has been reported [32–34].

The segregation of Cr, W and C in as-received state has been already observed in a similar ODS 14YWT [35] and in a 9Cr ODS steel [36].

According to S. Choudhury et al. [37], Cr has a relatively high diffusion coefficient through both interstitials and vacancies. Hence, a complicated combination of mechanisms may take place depending on the experimental conditions of the irradiation and the nature of the irradiated material.

According to T.R. Allen et al. [38], Cr segregation to grain boundaries has been systematically observed in irradiated ferritic martensitic steels; the maximum values being observed at 400 – 450°C for different alloys and irradiation conditions. The Cr segregation to grain boundaries displayed in Fig. 7 agrees with this observation.

Oversized solute atoms, like W, tend to deplete at the grain boundary under irradiation [39]. In this study, radiation-induced segregation of W to the grain boundaries has been observed, although not as distinctly in comparison with Cr and C. C. Parish et al. [14] also observed W segregation to grain boundaries in heavy ion irradiated 14YWT.

C segregation to grain boundaries is also evident in our study (Fig. 7), even though this observation is rarely reported in the literature [40]. Carbide formation can be promoted under irradiation, and grain boundaries are favorable sites for it [41]. In our case, carbide precipitation is not inferred from the 3D map (Fig. 2) and 1D analysis performed (Fig. 7). C enrichment can come from partial dissolution of carbides present in the material, frequently observed in ODS alloys [26] but not found in the APT datasets analyzed in this study. Also, a definitive outcome on this point cannot be made due to the nanometric sampling volumes

reconstructed by APT. The increased enrichment observed at the grain boundaries could also be the result of carbon contamination, a possibility with ion irradiations, but detailed design of experiments and analysis such as those performed in [42], were not completed at the time of this study.

Segregation of elements to the grain boundaries together with an increase in the number density of nanoparticles after irradiation seem to be the most significant irradiation induced effect on the microstructure of the 14YWT alloy, which may affect the mechanical properties. However, micromechanical testing results recently reported on the same heat of 14YWT [18] showed that it was resistant to irradiation hardening, as similar hardness and modulus profiles were measured before and after irradiation as well as a function of depth in cross section measurements. D.T. Hoelzer et al. [43] reported that the segregation of interstitial elements to grain boundaries in as-received 14YWT lowered the fracture toughness at elevated temperatures by decreasing the cohesive energy between grains that allowed for easy crack propagation. Whether the radiation induced segregation observed for 14YWT in this study affected the fracture toughness cannot be ascertained since fracture toughness samples were not part of the irradiation program.

Conclusions

The ODS 14YWT alloy (SM13) has been characterized at the nanoscale in as-received state and after an ion irradiation experiment using 70 MeV Fe^{9+} ions at 450°C (21 dpa total dose).

The main irradiation induced effects observed in this study are: increase of the number density of nanoparticles and radiation induced segregation to grain boundaries. The following conclusions can be drawn:

- Y-Ti-O rich nanoparticles are found decorating grain boundaries and within grains, being larger **in or close to** the grain boundaries.
- The nanoparticle size remains unchanged after irradiation, **both inside grains and at grain boundaries**.
- The number density of nanoclusters is lower at grain boundaries than inside grains in the as-received state, but this value increases in both locations after irradiation, with a higher increase being observed **in or close to** the grain boundaries. Also, the clusters are found to be closer together after irradiation.
- The Y:Ti ratio increases after irradiation while the (Y+Ti):O ratio remains constant.
- Cr, W and C segregation to the grain boundaries is observed in the as-received state.

Enhanced segregation of these elements induced by the irradiation is apparent.

The observations in this work, together with unchanged mechanical properties recently reported in [18] suggest that this alloy is stable to the given irradiation conditions, so it can remain as a promising candidate for use in Gen IV nuclear reactors.

Acknowledgements

Funding from US-DOE NEUP IRP (DE-NE0000639), UK-EP SRC (grants EP/P001645/1, EP/L025817/1 and EP/M022803/1) and Comunidad Autónoma de Madrid-Spain (2017-T1/IND-5439) is acknowledged. Part of the FIB sample preparation used UKAEA's Materials Research Facility, which has been funded by and is part of the UK's National Nuclear User Facility and Henry Royce Institute for Advanced Materials. Dr Scott J. Tumey is gratefully acknowledged for conducting the irradiation experiment at CAMS-LLNL.

Data availability

The raw/processed data required to reproduce these findings cannot be shared at this time due to technical or time limitations.

References

- [1] S. Ukai, M. Fujiwara, Perspective of ODS alloys application in nuclear environments, *J. Nucl. Mater.* (2002). doi:10.1016/S0022-3115(02)01043-7.
- [2] L.K. Mansur, A.F. Rowcliffe, R.K. Nanstad, S.J. Zinkle, W.R. Corwin, R.E. Stoller, Materials needs for fusion, Generation IV fission reactors and spallation neutron sources - Similarities and differences, in: *J. Nucl. Mater.*, 2004. doi:10.1016/j.jnucmat.2004.04.016.
- [3] G.R. Odette, M.J. Alinger, B.D. Wirth, Recent Developments in Irradiation-Resistant Steels, *Annu. Rev. Mater. Res.* (2008). doi:10.1146/annurev.matsci.38.060407.130315.
- [4] Z. Oksiuta, N. Baluc, Optimization of the chemical composition and manufacturing route for ODS RAF steels for fusion reactor application, *Nucl. Fusion.* (2009). doi:10.1088/0029-5515/49/5/055003.
- [5] S.J. Zinkle, J.T. Busby, Structural materials for fission & fusion energy, *Mater. Today.* (2009). doi:10.1016/S1369-7021(09)70294-9.
- [6] A. Hirata, T. Fujita, Y.R. Wen, J.H. Schneibel, C.T. Liu, M.W. Chen, Atomic structure of nanoclusters in oxide-dispersion-strengthened steels, *Nat. Mater.* (2011). doi:10.1038/nmat3150.
- [7] S.J. Zinkle, J.L. Boutard, D.T. Hoelzer, A. Kimura, R. Lindau, G.R. Odette, M. Rieth, L. Tan, H. Tanigawa, Development of next generation tempered and ODS reduced activation ferritic/martensitic steels for fusion energy applications, *Nucl. Fusion.* (2017). doi:10.1088/1741-4326/57/9/092005.
- [8] S.J. Zinkle, N.M. Ghoniem, Operating temperature windows for fusion reactor structural materials, *Fusion Eng. Des.* (2000). doi:10.1016/S0920-3796(00)00320-3.
- [9] J.P. Wharry, M.J. Swenson, K.H. Yano, A review of the irradiation evolution of dispersed oxide nanoparticles in the b.c.c. Fe-Cr system: Current understanding and future directions, *J. Nucl. Mater.* 486 (2017) 11–20. doi:10.1016/j.jnucmat.2017.01.009.
- [10] D.A. McClintock, M.A. Sokolov, D.T. Hoelzer, R.K. Nanstad, Mechanical properties of irradiated ODS-EUROFER and nanocluster strengthened 14YWT, *J. Nucl. Mater.* 392 (2009) 353–359. doi:10.1016/j.jnucmat.2009.03.024.
- [11] A. Certain, S. Kuchibhatla, V. Shutthanandan, D.T. Hoelzer, T.R. Allen, Radiation stability of nanoclusters in nano-structured oxide dispersion strengthened (ODS) steels, *J. Nucl. Mater.* 434 (2013) 311–321. doi:10.1016/j.jnucmat.2012.11.021.

- [12] M. Šćepanović, T. Leguey, M.A. Auger, S. Lozano-Perez, D.E.J. Armstrong, I. García-Cortés, V. de Castro, Characterisation of ODS Fe-14Cr-2W-0.3Ti before and after high temperature triple and low temperature single ion irradiations, *Mater. Charact.* (2018). doi:10.1016/j.matchar.2017.12.025.
- [13] R. Hu, G.D.W. Smith, E.A. Marquis, Effect of grain boundary orientation on radiation-induced segregation in a Fe-15.2 at.% Cr alloy, *Acta Mater.* (2013). doi:10.1016/j.actamat.2013.02.043.
- [14] C.M. Parish, R.M. White, J.M. LeBeau, M.K. Miller, Response of nanostructured ferritic alloys to high-dose heavy ion irradiation, *J. Nucl. Mater.* 445 (2014) 251–260. doi:10.1016/J.JNUCMAT.2013.11.002.
- [15] C. Zheng, M.A. Auger, M.P. Moody, D. Kaoumi, Radiation induced segregation and precipitation behavior in self-ion irradiated Ferritic/Martensitic HT9 steel, *J. Nucl. Mater.* (2017). doi:10.1016/j.jnucmat.2017.04.040.
- [16] M. Song, C.R. Lear, C.M. Parish, M. Wang, G.S. Was, Radiation tolerance of commercial and advanced alloys for core internals: a comprehensive microstructural characterization, *J. Nucl. Mater.* 510 (2018) 396–413. doi:10.1016/j.jnucmat.2018.08.035.
- [17] D.T. Hoelzer, K.A. Unocic, W. Tang, Z. Feng, Status of joining thin sheet and thin wall tubes of 14YWT (No. ORNL/TM-2015/548), 2015. <https://info.ornl.gov/sites/publications/Files/Pub59258.pdf>.
- [18] A. Prasitthipayong, D. Frazer, A. Kareer, M.D. Abad, A. Garner, B. Joni, T. Ungar, G. Ribarik, M. Preuss, L. Balogh, S.J. Tumey, A.M. Minor, P. Hosemann, Micro mechanical testing of candidate structural alloys for Gen-IV nuclear reactors, *Nucl. Mater. Energy.* 16 (2018) 34–45. doi:10.1016/j.nme.2018.05.018.
- [19] J.F. Ziegler, M.D. Ziegler, J.P. Biersack, SRIM - The stopping and range of ions in matter (2010), *Nucl. Instruments Methods Phys. Res. Sect. B Beam Interact. with Mater. Atoms.* (2010). doi:10.1016/j.nimb.2010.02.091.
- [20] M.K. Miller, K.F. Russell, K. Thompson, R. Alvis, D.J. Larson, Review of atom probe FIB-based specimen preparation methods, in: *Microsc. Microanal.*, 2007. doi:10.1017/S1431927607070845.
- [21] M.K. Miller, *Atom probe tomography : analysis at the atomic level*, Kluwer Academic/Plenum Publishers, New York ; London, 2000.
- [22] C.A. Williams, D. Haley, E.A. Marquis, G.D.W. Smith, M.P. Moody, Defining clusters in APT reconstructions of ODS steels, *Ultramicroscopy.* (2013). doi:10.1016/j.ultramic.2012.12.011.
- [23] M.K. Miller, R. Forbes, ProQuest (Firm), *Atom probe tomography : the local electrode atom probe*, (2014) 1 online resource (437 pages).
- [24] M.K. Miller, E.A. Kenik, *Atom probe tomography: A technique for nanoscale characterization*, in: *Microsc. Microanal.*, 2004. doi:10.1017/S1431927604040577.

- [25] R.S. Nelson, J.A. Hudson, D.J. Mazey, The stability of precipitates in an irradiation environment, *J. Nucl. Mater.* 44 (1972) 318–330. doi:10.1016/0022-3115(72)90043-8.
- [26] V. de Castro, T. Leguey, M.A. Auger, S. Lozano-Perez, M.L. Jenkins, Analytical characterization of secondary phases and void distributions in an ultrafine-grained ODS Fe–14Cr model alloy, *J. Nucl. Mater.* 417 (2011) 217–220. doi:10.1016/J.JNUCMAT.2010.12.067.
- [27] M.A. Auger, V. de Castro, T. Leguey, S. Lozano-Perez, P.A.J. Bagot, M.P. Moody, S.G. Roberts, Effect of the milling atmosphere on the microstructure and mechanical properties of a ODS Fe–14Cr model alloy, *Mater. Sci. Eng. A.* (2016). doi:10.1016/j.msea.2016.06.054.
- [28] D.A. Porter, K.E. Easterling, M.Y. Sherif, *Phase Transformations in Metals and Alloys*, Third Edition, 2009.
- [29] J. He, F. Wan, K. Sridharan, T.R. Allen, A. Certain, Y.Q. Wu, Response of 9Cr-ODS steel to proton irradiation at 400 °C, *J. Nucl. Mater.* (2014). doi:10.1016/j.jnucmat.2014.05.004.
- [30] J. He, F. Wan, K. Sridharan, T.R. Allen, A. Certain, V. Shutthanandan, Y.Q. Wu, Stability of nanoclusters in 14YWT oxide dispersion strengthened steel under heavy ion-irradiation by atom probe tomography, *J. Nucl. Mater.* (2014). doi:10.1016/j.jnucmat.2014.03.024.
- [31] M.J. Swenson, J.P. Wharry, The comparison of microstructure and nanocluster evolution in proton and neutron irradiated Fe–9%Cr ODS steel to 3 dpa at 500 °C, *J. Nucl. Mater.* (2015). doi:10.1016/j.jnucmat.2015.09.022.
- [32] G.S. Was, J.P. Wharry, B. Frisbie, B.D. Wirth, D. Morgan, J.D. Tucker, T.R. Allen, Assessment of radiation-induced segregation mechanisms in austenitic and ferritic–martensitic alloys, *J. Nucl. Mater.* 411 (2011) 41–50. doi:10.1016/j.jnucmat.2011.01.031.
- [33] Z. Jiao, G.S. Was, Segregation behavior in proton- and heavy-ion-irradiated ferritic–martensitic alloys, *Acta Mater.* (2011). doi:10.1016/j.actamat.2011.03.070.
- [34] V. de Castro, S. Lozano-Perez, M. Briceno, P. Trocellier, S.G. Roberts, R. Pareja, Effects of single- and simultaneous triple-ion-beam irradiation on an oxide dispersion-strengthened Fe12Cr steel, *J. Mater. Sci.* (2015). doi:10.1007/s10853-014-8794-y.
- [35] J.B. Seol, D. Haley, D.T. Hoelzer, J.H. Kim, Influences of interstitial and extrusion temperature on grain boundary segregation, Y–Ti–O nanofeatures, and mechanical properties of ferritic steels, *Acta Mater.* 153 (2018) 71–85. doi:10.1016/J.ACTAMAT.2018.04.046.
- [36] T.R. Allen, J. Gan, J.I. Cole, M.K. Miller, J.T. Busby, S. Shutthanandan, S. Thevuthasan, Radiation response of a 9 chromium oxide dispersion strengthened steel to heavy ion irradiation, *J. Nucl. Mater.* (2008). doi:10.1016/j.jnucmat.2007.11.001.
- [37] S. Choudhury, L. Barnard, J.D. Tucker, T.R. Allen, B.D. Wirth, M. Asta, D. Morgan, Ab-

initio based modeling of diffusion in dilute bcc Fe-Ni and Fe-Cr alloys and implications for radiation induced segregation, *J. Nucl. Mater.* (2011). doi:10.1016/j.jnucmat.2010.12.231.

- [38] T.R. Allen, D. Kaoumi, J.P. Wharry, Z. Jiao, C. Topbasi, A. Kohnert, L. Barnard, A. Certain, K.G. Field, G.S. Was, D.L. Morgan, A.T. Motta, B.D. Wirth, Y. Yang, Characterization of microstructure and property evolution in advanced cladding and duct: Materials exposed to high dose and elevated temperature, *J. Mater. Res.* (2015). doi:10.1557/jmr.2015.99.
- [39] A.J. Arderll, *Materials Issues for Generation IV Systems*, 2008. doi:10.1007/978-1-4020-8422-5.
- [40] R. Hu, G.D.W. Smith, E.A. Marquis, Atom probe study of radiation induced grain boundary segregation/depletion in a Fe-12%Cr alloy, in: *Prog. Nucl. Energy*, Pergamon, 2012: pp. 14–19. doi:10.1016/j.pnucene.2011.10.011.
- [41] C. Zheng, J.-H. Ke, S.A. Maloy, D. Kaoumi, Correlation of in-situ transmission electron microscopy and microchemistry analysis of radiation-induced precipitation and segregation in ion irradiated advanced ferritic/martensitic steels, *Scr. Mater.* 162 (2019) 460–464. doi:https://doi.org/10.1016/j.scriptamat.2018.12.018.
- [42] G.S. Was, S. Taller, Z. Jiao, A.M. Monterrosa, D. Woodley, D. Jennings, T. Kubley, F. Naab, O. Toader, E. Uberseder, Resolution of the carbon contamination problem in ion irradiation experiments, *Nucl. Instruments Methods Phys. Res. Sect. B Beam Interact. with Mater. Atoms.* (2017). doi:10.1016/j.nimb.2017.08.039.
- [43] D.T. Hoelzer, K.A. Unocic, M.A. Sokolov, T.S. Byun, Influence of processing on the microstructure and mechanical properties of 14YWT, *J. Nucl. Mater.* (2016). doi:10.1016/j.jnucmat.2015.12.011.

Tables

Table I. Bulk composition of as-received 14YWT (provided by ORNL) and APT results of bulk and matrix composition of as-received and **ion** irradiated 14YWT (at. %)

	Alloy Chemistry				
	ORNL results	14YWT as-received		14YWT irradiated	
	Bulk	Bulk	Matrix	Bulk	Matrix
Element	At. %	At. %	At. %	At. %	At. %
Fe	82.206	82.97 ± 0.72	83.13 ± 0.76	83.24 ± 1.12	83.47 ± 0.76
Cr	15.313	15.02 ± 0.42	15.05 ± 0.42	14.74 ± 0.31	15.15 ± 0.54
W	0.703	0.71 ± 0.18	0.75 ± 0.17	0.58 ± 0.24	0.52 ± 0.23
Ti	0.314	0.22 ± 0.10	0.14 ± 0.13	0.16 ± 0.06	0.06 ± 0.01
Y	0.119	0.12 ± 0.04	0.07 ± 0.05	0.11 ± 0.04	0.04 ± 0.04
O	0.616	0.46 ± 0.15	0.36 ± 0.18	0.51 ± 0.34	0.25 ± 0.15
N	0.394	0.17 ± 0.12	0.17 ± 0.12	0.15 ± 0.08	0.16 ± 0.06
C	0.111	0.15 ± 0.07	0.14 ± 0.07	0.42 ± 0.38	0.32 ± 0.37
Al	0.033	0.02 ± 0.02	0.02 ± 0.02	0.007 ± 0.006	0.006 ± 0.003
Si	0.085	0.08 ± 0.01	0.08 ± 0.02	0.05 ± 0.04	0.02 ± 0.02
P	0.016	0.005 ± 0.002	0.005 ± 0.002	0.003 ± 0.002	0.003 ± 0.002
Mn	0.008	0.02 ± 0.01	0.02 ± 0.01	0.02 ± 0.01	0.02 ± 0.01
Cu	0.030	0.04 ± 0.01	0.02 ± 0.02	0.001 ± 0.001	0.003 ± 0.003
Ni	0.011	0.018 ± 0.006	0.02 ± 0.01	0.007 ± 0.007	0.007 ± 0.007
S	0.005	----	----	----	----
Nb	0.001	----	----	----	----
Mo	0.000	----	----	----	----
Co	0.035	----	----	----	----

Table II. Summary of the cluster analysis statistics.

	Clusters inside grains		Clusters in or close to grain boundaries	
	14YWT as-received	14YWT irradiated	14YWT as-received	14YWT irradiated
Number of clusters	1104	327	742	924
Cluster size range (nm)	0.76 - 4.85	0.62 - 3.60	0.82 - 8.37	0.37 -9.34
Median cluster size (nm)	1.64	1.74	2.19	2.13
Average cluster size (nm)	1.74 ± 0.59	1.75 ± 0.49	2.21 ± 0.86	2.29 ± 0.90
Number density of clusters ($\times 10^{24} \text{ m}^{-3}$)	1.49 ± 0.25	2.08 ± 0.71	0.94 ± 0.69	1.37 ± 0.87
Distance between nearest neighbor clusters (nm)	6.82 ± 2.60	6.52 ± 2.19	7.24 ± 3.10	7.02 ± 2.25

Table III. Summary of the cluster composition.

	Clusters inside grains		Clusters in or close to grain boundaries	
	14YWT as-received	14YWT irradiated	14YWT as-received	14YWT irradiated
Y (at. %)	26.83 ± 8.36	30.66 ± 7.29	27.01 ± 8.07	31.78 ± 8.38
Ti (at. %)	32.75 ± 5.49	28.95 ± 5.30	31.94 ± 5.63	27.35 ± 6.69
O (at. %)	40.42 ± 3.74	40.39 ± 3.44	41.04 ± 3.29	40.87 ± 3.50
Y:Ti	0.91 ± 0.69	1.16 ± 0.62	0.94 ± 0.74	1.38 ± 1.10
(Y+Ti):O	1.50 ± 0.31	1.50 ± 0.24	1.45 ± 0.23	1.47 ± 0.26

Table IV. Summary of peak composition and interface width at the grain boundaries.

	14YWT as-received	14YWT irradiated
C (at. %)	0.47 ± 0.15	3.97 ± 1.58
W (at. %)	1.20 ± 0.43	1.31 ± 0.64
Cr (at. %)	19.91 ± 1.48	25.37 ± 4.13
Interface width (nm)	11.02 ± 3.60	8.80 ± 2.00
Number of analyzed interfaces	5	10

Figure legends

Fig. 1. (a) Extruded bar containing consolidated 14YWT. (b) Cross-rolled plate enclosed in mild steel can. (c) De-canned cross-rolled plate.

Fig. 2. 3D ion maps of as-received 14YWT showing (a) volume inside a grain and (b) volume containing grain boundaries.

Fig. 3. 3D ion maps of ion irradiated 14YWT showing a) volume inside a grain and b) volume containing grain boundaries.

Fig. 4. Size (Guinier diameter) distribution of clusters (a) inside grains and (b) at grain boundaries in as-received 14YWT and (c) inside grains and (d) **in or close to** grain boundaries in ion irradiated 14YWT.

Fig. 5. Chemistry of the clusters inside grains for 14YWT (a) as-received and (b) ion irradiated and **in or close to** grain boundaries for 14YWT (c) as-received and (d) ion irradiated.

Fig. 6. 1D chemical analysis through one grain boundary in as-received 14YWT.

Fig. 7. 1D chemical analysis through one grain boundary in irradiated 14YWT.

Additional data

Fig. 8. Additional datasets of volumes inside grains in as-received 14YWT.

Fig. 9. Additional datasets of volumes containing grain boundaries in as-received 14YWT.

Fig. 10. Additional datasets of volumes inside grains in irradiated 14YWT.

Fig. 11. Additional datasets of volumes containing grain boundaries in irradiated 14YWT.

Nanoscale analysis of ion irradiated ODS 14YWT ferritic alloy

Maria A. Auger^{1,2*}, David T. Hoelzer³, Kevin G. Field³, Michael P. Moody²

¹Physics Department, Universidad Carlos III de Madrid. Avenida Universidad 30, 28911 Leganés, Madrid, Spain.

²Department of Materials, University of Oxford. Parks Road OX1 3PH, Oxford, UK.

³Oak Ridge National Laboratory, Oak Ridge, TN 37831, Tennessee, USA.

*Corresponding Author: Tel. +34 91 624 9478, Fax. +34 91 624 8749, e-mail address:

mauger@fis.uc3m.es

Abstract

In this work, the nanoscale microstructure of an advanced oxide dispersion strengthened (ODS) 14YWT ferritic alloy (SM13 heat) with nominal composition Fe-14Cr-3W-0.4Ti-0.3Y₂O₃ (wt. %) has been characterized by atom probe tomography (APT) before and after ion irradiation with 70 MeV Fe⁹⁺ ions at 450°C to a total dose of 21 dpa. A detailed solute cluster analysis of APT data reveals that, in the manufacturing process, larger nanoparticles form in or close to the grain boundaries respective to those inside grains. The evolution of the nanoparticles after irradiation seems to be related to their location, as a higher increase in the number density and in the Y:Ti ratio is observed for the nanoparticles in or close to grain boundaries. APT analysis also shows Cr, W and C segregation to grain boundaries enhanced by the irradiation. A previous study of this same alloy before and after irradiation reports that the mechanical properties do not seem to be affected, but the microstructure was not investigated to confirm. The present work confirms little microstructural evolution after irradiation in this 14YWT alloy, indicating tolerance at the given irradiation conditions.

Keywords

14YWT, ODS alloys, atom probe tomography, ion irradiation, clusters

Introduction

Oxide dispersion strengthened (ODS) steels and ferritic alloys have remained candidate structural materials for nuclear applications in Gen IV and fusion reactors over the last decade due to the dispersion of nano-size oxide particles (nanoparticles) improving their mechanical performance and radiation tolerance [1–7]. The presence of nanoparticles plays an essential role in these behaviors by impeding dislocation motion and cavity growth, which in turn enhances the creep resistance while simultaneously reducing the impacts of irradiation. The nanoparticle dispersion thus allows for exposure to increased operating temperatures and radiation dose regimes compared to conventional ferritic alloys [8]. Results from a variety of experimental conditions, including different manufacturing routes, alloy compositions and irradiation parameters, have been recently summarized by J. Wharry et al. in [9] and, apart from experimental differences, the ODS alloys generally show resistance under irradiation for typical operating conditions of nuclear power reactors in terms of microstructural evolution and radiation-induced hardening. For instance, D.A. McClintock et al. [10] characterized 14YWT exposed to 1.5 dpa neutron irradiation at 300 – 750°C and found good resistance to radiation-induced hardening. This was attributed to the fine grain structure and high number density of nanoclusters in the alloy. A. Certain et al. [11] studied a 14YWT alloy (SM10 heat), similar to the alloy presented in this work, irradiated with protons (to 1 and 3 dpa at 400°C) and Ni²⁺ ions (to 50 and 100 dpa from - 75°C to 600°C). They observed dissolution of the nanoclusters after heavy-ion irradiation at

cryogenic temperatures, while little to no changes were observed in samples irradiated at reactor relevant conditions (600°C). M. Šćepanović et al. [12] submitted a 14YWTi alloy to triple ion (Fe^{5+} , He^+ and H^+) irradiation at 600°C and to single ion (Fe^{5+}) irradiation at -80°C, and confirmed the stability of the nanoparticles after both irradiation experiments, with only slight differences regarding the size and composition of the nanoparticles observed. However, as highlighted in [9], even though results from a large number of studies are available, there is a high difficulty in normalizing these observations across the wide range of irradiation sources, dose rates, temperatures and different compositions of irradiated ODS alloys that have been investigated. Hence, clear conclusions regarding the evolution of the nanoparticles under irradiation at common nuclear power reactor temperatures have yet to be established. A similar observation can be made regarding radiation induced segregation in high chromium Fe-based body-centered cubic alloys. The literature provides a wide range of studies [13–16], but a clear conclusion cannot be reached, as segregation and depletion of solute atom concentration to specific regions of the microstructure have been reported, along with other cases where no apparent change is observed. Therefore, further experimental and theoretical studies are needed in order to understand and predict the evolution of these alloys under irradiation.

The aim of this work is to contribute to that effort by characterizing the nanoscale microstructure of the advanced ODS 14YWT ferritic alloy (SM13 heat) with nominal composition Fe-14Cr-3W-0.4Ti-0.3Y₂O₃ (wt. %), before and after irradiation with a high energy (70 MeV) Fe^{9+} ion beam to 21 dpa at 450°C. The atom probe tomography (APT) characterization technique has been used to perform a detailed cluster analysis and radiation induced segregation (RIS) effects study.

Materials and Methods

The ODS 14YWT ferritic alloy (SM13 heat) was produced by mechanical alloying at Oak Ridge National Laboratory (ORNL) [17]. Gas atomized powder (Special Metals, Inc.) of composition Fe-14Cr-3W-0.4Ti (wt. %) was ball milled with 0.3 wt.% Y₂O₃ powder (Nanophase, Inc.) using a high kinetic energy CM08 Simoloyer (Zoz, GmbH) for 40 h in Ar atmosphere. The milled powder was canned in mild steel, degassed for 24 h at 300°C under vacuum and consolidated by hot extrusion through a rectangular-shaped die after a heat treatment of 1 h at 850°C. A plate was produced from the extruded bar by cross rolling at 1000°C, reaching a 50% reduction in thickness. The mild steel can was kept on the extruded ODS 14YWT bar during cross rolling to avoid additional contamination. Images of the sample at different stages can be seen in Fig. 1. The C and S bulk composition was measured by combustion infrared detection, the O and N was determined from inert gas fusion, while all other alloying elements bulk composition was determined using direct current plasma emission spectroscopy. Table I summarizes the resulting bulk composition analysis performed by ORNL together with the average bulk and matrix compositions obtained from APT analysis (8 datasets for the as-received 14YWT sample and 7 datasets for the ion irradiated sample). The irradiation experiment was held at the Center of Accelerator Mass Spectrometry (CAMS), Lawrence Livermore National Laboratory (LLNL), CA using a rastered beam of 70 MeV Fe⁹⁺ ions to a total accumulated dose of 21 dpa and dose rate of 3.7×10^{-4} dpa/s at a nominal temperature of 450°C (the original dose is 20.68, as quoted by A. Prasitthipayong et al. in [18]). The actual temperature, monitored by an IR camera and a thermocouple behind the sample, was 456 ± 11 °C averaged over the 15.55 h irradiation time. The average current was 19.47 nC/s, measured using an array of micro Faraday cups. SRIM simulations [19], using a displacement energy of 40 eV and a ion flux value of 10^{15} ions/cm² in the modified

Kinchin–Pease model of the SRIM-2013 software version were made. These calculations predict that the damage layer will extend approximately to a depth of 6.2 μm from the sample surface [18].

Needle-shaped samples for atom probe characterization were prepared by the lift-out method [20] using three dual beam FIB/SEM instruments: a FEI Helios NanoLab 600i at the Materials Research Facility (MRF) in Culham Center for Fusion Energy (CCFE), and a Zeiss Auriga 40 and a Zeiss NVision 40 at the Department of Materials, University of Oxford. The APT analysis was performed at the Department of Materials, University of Oxford. A CAMECA LEAP™ 3000X HR in laser mode ($\lambda = 532 \text{ nm}$, 0.40 nJ laser energy) at a repetition rate of 200 kHz and a CAMECA LEAP™ 5000XR operating in laser mode ($\lambda = 355 \text{ nm}$, 0.040 – 0.050 nJ laser energy) at a repetition rate of 200 kHz were used; the sample temperature was always kept at 50 – 55K. A total of 15 high quality datasets, containing between 1 and 30 million ions, were analyzed. CAMECA IVAS™ software together with Origin®, MATLAB® and Corel® Photo-Paint® were used to produce the results and figures in this work. The analyzed volumes were reconstructed by setting shank angles and tip radii values from SEM images of the FIB prepared samples. The cluster analysis was made by implementing the maximum separation method [21]; this method defines clusters by setting a minimum number of ions, N_{min} , separated from each other a distance shorter than d_{max} . The cluster selection parameters, N_{min} and d_{max} , for each dataset were defined according to the criteria developed in [22]. The cluster size was calculated as the Guinier diameter, i.e. twice the Guinier radius [23]; and the distance between clusters was taken as the average distance between the center of mass [24] of one cluster and the center of mass of its first neighbor.

Results

Reconstructed 3D maps showing the Y, Y-O and Ti-O ion distributions in the as-received and irradiated 14YWT alloy are shown in Figs. 2 and 3, respectively. C ion maps are also included to highlight the presence of grain boundaries, as C was found to segregate to grain boundaries in both the as-received and irradiated conditions. Ion map reconstructions from all the datasets used in this study are included as Supplementary material. As the size of the oxygen-enriched clusters within the grains may be different from those in or close to grain boundaries, they were analyzed separately by splitting the datasets into customized regions of interest (ROI) containing the relevant volumes.

The size distribution of clusters is shown in Fig. 4, and a summary of the cluster analysis statistics is included in Table II. In the as-received sample, clusters in or close to the grain boundaries are 27 % larger than those inside grains and, in the irradiated sample, this difference in size is 31 %. On the other hand, the average size of the clusters inside grains is very similar in the as received and irradiated states, respectively, of 14YWT, and a similar observation can be made when comparing the clusters in or close to grain boundaries.

A 40 % and 46 % increase in the average number density of nanoparticles after irradiation can be observed respectively inside grains and in or close to grain boundaries (Table II).

In addition, the cluster separation distance was found to be 4% and 3% closer in the irradiated state compared to the as-received sample, respectively inside grains and in or close to grain boundaries (Table II).

Regarding the cluster composition, the chemistry of all the analyzed clusters is graphically displayed in Fig. 5 and summarized in Table III. In this case, a variation in the Y and Ti content can be observed in the irradiated state compared to the as-received condition, with average Y content increasing and Ti content decreasing. It is worth noting that there is a

large variation of stoichiometry in the analyzed clusters, especially in the smaller ones, as it has been observed in previous studies [11,12].

The Y:Ti ratio after irradiation increases in the clusters located inside grains and in or close to grain boundaries by 27% and 47%, respectively. The (Y+Ti):O ratio remains almost constant, in the 1.44 – 1.48 narrow range, for all the analyzed clusters.

An important radiation effect is the segregation of elements (Cr, W and C) to grain boundaries. Figs. 6 and 7, show 1D elemental concentration analysis across grain boundary interfaces for the as-received and irradiated samples, respectively. The peak compositions for each element are summarized in Table IV. Peak at. % concentration values for Cr and W are 27% and 9% higher after irradiation, respectively. C segregation is highly enhanced by the irradiation, with a peak value 8.4 times higher than in the as-received state. The size of the segregation interface is measured as the distance between minimum concentration values around the segregation peak. The interface width was observed to be 20% narrower in the irradiated state compared to the as-received sample (Table IV).

Discussion

Cluster analysis

Distinction of cluster behavior after irradiation by considering their location, inside grains and in or close to grain boundaries, is not usually considered in the literature. In our study, differences in the nanocluster evolution are apparent depending on their location in the microstructure. In the as-received alloy, nanoparticles in or close to grain boundaries are larger than those inside grains, but their size remains unchanged after irradiation at both locations. The number density of nanoclusters is lower in or close to grain boundaries than

inside grains in the as-received state. After irradiation, this value increases in both locations and the clusters are found to be closer together.

As reported in [9], there is a large variation of results regarding the evolution of nanoparticles in ODS steels under irradiation, making it very difficult to establish a specific mechanism describing the effects of irradiation taking place. Actually, a combination of several mechanisms including ballistic dissolution, Ostwald ripening and irradiation-enhanced diffusion seem to justify the observed evolution of clusters in irradiated ODS steels.

By ballistic dissolution [25] atoms can be ejected from clusters as a consequence of the ballistic collisions from irradiation damage cascades. APT sample volumes typically contain clusters < 10 nm in size, but TEM studies usually report the presence of larger clusters in ODS alloys [26,27]; these larger clusters would be more likely to follow ballistic dissolution for being a bigger cross-sectional target. The ejected atoms can subsequently diffuse back into the initial cluster, diffuse to a different cluster or diffuse into the matrix. Those diffusing into the matrix can initiate homogeneous nucleation (inside grains) or heterogeneous nucleation (at grain boundaries or other defects), with this last one being more energetically favorable [28]. Nanoparticles that are nucleated from the ejected solutes will grow until reaching a steady-state size determined by the balance in flux of solutes being ejected and attached. In our study, there is an increase of 46% in the number density of clusters in or close to grain boundaries compared to the 40% increase for clusters inside the grains. Also, the nanoparticle size after irradiation is very similar to the nanoparticle size in unirradiated state.

The Y:Ti ratio increases after irradiation, consistent with other studies in the literature [29–31], suggesting that Ti atoms are more easily displaced from nanoclusters than Y atoms and,

in our specific case, Ti atoms are more prone to displace in or close to grain boundaries than inside grains.

The (Y + Ti):O ratio remains constant; this observation may confirm that the displacement of O atoms and ejection of Ti atoms take place at the same rate [31].

Dissolution, nucleation and coarsening mechanisms act simultaneously during irradiation and, according to the experimental results presented here, they seem to happen at different rates inside grains and in or close to grain boundaries.

Radiation-induced segregation

Radiation-induced segregation (RIS) is known to be a non-equilibrium process which produces point defects that, depending on the irradiation temperature, can be mobile and relocate to defect sinks like surfaces, grain boundaries or dislocations [32]. Components which diffuse more quickly via interstitials will tend to segregate to grain boundaries, while components which diffuse more quickly via vacancies will tend to deplete.

A specific trend regarding radiation-induced segregation of elements in irradiated ODS steels cannot be found in the literature, as both segregation, depletion or no change of elements to grain boundaries and dislocations has been reported [32–34].

The segregation of Cr, W and C in as-received state has been already observed in a similar ODS 14YWT [35] and in a 9Cr ODS steel [36].

According to S. Choudhury et al. [37], Cr has a relatively high diffusion coefficient through both interstitials and vacancies. Hence, a complicated combination of mechanisms may take place depending on the experimental conditions of the irradiation and the nature of the irradiated material.

According to T.R. Allen et al. [38], Cr segregation to grain boundaries has been systematically observed in irradiated ferritic martensitic steels; the maximum values being observed at 400 – 450°C for different alloys and irradiation conditions. The Cr segregation to grain boundaries displayed in Fig. 7 agrees with this observation.

Oversized solute atoms, like W, tend to deplete at the grain boundary under irradiation [39].

In this study, radiation-induced segregation of W to the grain boundaries has been observed, although not as distinctly in comparison with Cr and C. C. Parish et al. [14] also observed W segregation to grain boundaries in heavy ion irradiated 14YWT.

C segregation to grain boundaries is also evident in our study (Fig. 7), even though this observation is rarely reported in the literature [40]. Carbide formation can be promoted under irradiation, and grain boundaries are favorable sites for it [41]. In our case, carbide precipitation is not inferred from the 3D map (Fig. 2) and 1D analysis performed (Fig. 7). C enrichment can come from partial dissolution of carbides present in the material, frequently observed in ODS alloys [26] but not found in the APT datasets analyzed in this study. Also, a definitive outcome on this point cannot be made due to the nanometric sampling volumes reconstructed by APT. The increased enrichment observed at the grain boundaries could also be the result of carbon contamination, a possibility with ion irradiations, but detailed design of experiments and analysis such as those performed in [42], were not completed at the time of this study.

Segregation of elements to the grain boundaries together with an increase in the number density of nanoparticles after irradiation seem to be the most significant irradiation induced effect on the microstructure of the 14YWT alloy, which may affect the mechanical properties. However, micromechanical testing results recently reported on the same heat of 14YWT [18] showed that it was resistant to irradiation hardening, as similar hardness and

modulus profiles were measured before and after irradiation as well as a function of depth in cross section measurements. D.T. Hoelzer et al. [43] reported that the segregation of interstitial elements to grain boundaries in as-received 14YWT lowered the fracture toughness at elevated temperatures by decreasing the cohesive energy between grains that allowed for easy crack propagation. Whether the radiation induced segregation observed for 14YWT in this study affected the fracture toughness cannot be ascertained since fracture toughness samples were not part of the irradiation program.

Conclusions

The ODS 14YWT alloy (SM13) has been characterized at the nanoscale in as-received state and after an ion irradiation experiment using 70 MeV Fe^{9+} ions at 450°C (21 dpa total dose). The main irradiation induced effects observed in this study are: increase of the number density of nanoparticles and radiation induced segregation to grain boundaries. The following conclusions can be drawn:

- Y-Ti-O rich nanoparticles are found decorating grain boundaries and within grains, being larger in or close to the grain boundaries.
- The nanoparticle size remains unchanged after irradiation.
- The number density of nanoclusters is lower at grain boundaries than inside grains in the as-received state, but this value increases in both locations after irradiation, with a higher increase being observed in or close to the grain boundaries. Also, the clusters are found to be closer together after irradiation.
- The Y:Ti ratio increases after irradiation while the (Y+Ti):O ratio remains constant.
- Cr, W and C segregation to the grain boundaries is observed in the as-received state.

Enhanced segregation of these elements induced by the irradiation is apparent.

The observations in this work, together with unchanged mechanical properties recently reported in [18] suggest that this alloy is stable to the given irradiation conditions, so it can remain as a promising candidate for use in Gen IV and fusion reactors.

Acknowledgements

Funding from US-DOE NEUP IRP (DE-NE0000639), UK-EP SRC (grants EP/P001645/1, EP/L025817/1 and EP/M022803/1) and Comunidad Autónoma de Madrid-Spain (2017-T1/IND-5439) is acknowledged. Part of the FIB sample preparation used UKAEA's Materials Research Facility, which has been funded by and is part of the UK's National Nuclear User Facility and Henry Royce Institute for Advanced Materials. Dr Scott J. Tumey is gratefully acknowledged for conducting the irradiation experiment at CAMS-LLNL.

Data availability

The raw/processed data required to reproduce these findings cannot be shared at this time due to technical or time limitations.

References

- [1] S. Ukai, M. Fujiwara, Perspective of ODS alloys application in nuclear environments, *J. Nucl. Mater.* (2002). doi:10.1016/S0022-3115(02)01043-7.
- [2] L.K. Mansur, A.F. Rowcliffe, R.K. Nanstad, S.J. Zinkle, W.R. Corwin, R.E. Stoller, Materials needs for fusion, Generation IV fission reactors and spallation neutron sources - Similarities and differences, in: *J. Nucl. Mater.*, 2004. doi:10.1016/j.jnucmat.2004.04.016.
- [3] G.R. Odette, M.J. Alinger, B.D. Wirth, Recent Developments in Irradiation-Resistant Steels, *Annu. Rev. Mater. Res.* (2008). doi:10.1146/annurev.matsci.38.060407.130315.
- [4] Z. Oksiuta, N. Baluc, Optimization of the chemical composition and manufacturing route for ODS RAF steels for fusion reactor application, *Nucl. Fusion.* (2009). doi:10.1088/0029-5515/49/5/055003.

- [5] S.J. Zinkle, J.T. Busby, Structural materials for fission & fusion energy, *Mater. Today*. (2009). doi:10.1016/S1369-7021(09)70294-9.
- [6] A. Hirata, T. Fujita, Y.R. Wen, J.H. Schneibel, C.T. Liu, M.W. Chen, Atomic structure of nanoclusters in oxide-dispersion-strengthened steels, *Nat. Mater.* (2011). doi:10.1038/nmat3150.
- [7] S.J. Zinkle, J.L. Boutard, D.T. Hoelzer, A. Kimura, R. Lindau, G.R. Odette, M. Rieth, L. Tan, H. Tanigawa, Development of next generation tempered and ODS reduced activation ferritic/martensitic steels for fusion energy applications, *Nucl. Fusion*. (2017). doi:10.1088/1741-4326/57/9/092005.
- [8] S.J. Zinkle, N.M. Ghoniem, Operating temperature windows for fusion reactor structural materials, *Fusion Eng. Des.* (2000). doi:10.1016/S0920-3796(00)00320-3.
- [9] J.P. Wharry, M.J. Swenson, K.H. Yano, A review of the irradiation evolution of dispersed oxide nanoparticles in the b.c.c. Fe-Cr system: Current understanding and future directions, *J. Nucl. Mater.* 486 (2017) 11–20. doi:10.1016/j.jnucmat.2017.01.009.
- [10] D.A. McClintock, M.A. Sokolov, D.T. Hoelzer, R.K. Nanstad, Mechanical properties of irradiated ODS-EUROFER and nanocluster strengthened 14YWT, *J. Nucl. Mater.* 392 (2009) 353–359. doi:10.1016/j.jnucmat.2009.03.024.
- [11] A. Certain, S. Kuchibhatla, V. Shutthanandan, D.T. Hoelzer, T.R. Allen, Radiation stability of nanoclusters in nano-structured oxide dispersion strengthened (ODS) steels, *J. Nucl. Mater.* 434 (2013) 311–321. doi:10.1016/j.jnucmat.2012.11.021.
- [12] M. Šćepanović, T. Leguey, M.A. Auger, S. Lozano-Perez, D.E.J. Armstrong, I. García-Cortés, V. de Castro, Characterisation of ODS Fe-14Cr-2W-0.3Ti before and after high temperature triple and low temperature single ion irradiations, *Mater. Charact.* (2018). doi:10.1016/j.matchar.2017.12.025.
- [13] R. Hu, G.D.W. Smith, E.A. Marquis, Effect of grain boundary orientation on radiation-induced segregation in a Fe-15.2 at.% Cr alloy, *Acta Mater.* (2013). doi:10.1016/j.actamat.2013.02.043.
- [14] C.M. Parish, R.M. White, J.M. LeBeau, M.K. Miller, Response of nanostructured ferritic alloys to high-dose heavy ion irradiation, *J. Nucl. Mater.* 445 (2014) 251–260. doi:10.1016/J.JNUCMAT.2013.11.002.
- [15] C. Zheng, M.A. Auger, M.P. Moody, D. Kaoumi, Radiation induced segregation and precipitation behavior in self-ion irradiated Ferritic/Martensitic HT9 steel, *J. Nucl. Mater.* (2017). doi:10.1016/j.jnucmat.2017.04.040.
- [16] M. Song, C.R. Lear, C.M. Parish, M. Wang, G.S. Was, Radiation tolerance of commercial and advanced alloys for core internals: a comprehensive microstructural characterization, *J. Nucl. Mater.* 510 (2018) 396–413. doi:10.1016/j.jnucmat.2018.08.035.
- [17] D.T. Hoelzer, K.A. Unocic, W. Tang, Z. Feng, Status of joining thin sheet and thin wall

tubes of 14YWT (No. ORNL/TM-2015/548), 2015.
<https://info.ornl.gov/sites/publications/Files/Pub59258.pdf>.

- [18] A. Prasitthipayong, D. Frazer, A. Kareer, M.D. Abad, A. Garner, B. Joni, T. Ungar, G. Ribarik, M. Preuss, L. Balogh, S.J. Tumey, A.M. Minor, P. Hosemann, Micro mechanical testing of candidate structural alloys for Gen-IV nuclear reactors, *Nucl. Mater. Energy*. 16 (2018) 34–45. doi:10.1016/j.nme.2018.05.018.
- [19] J.F. Ziegler, M.D. Ziegler, J.P. Biersack, SRIM - The stopping and range of ions in matter (2010), *Nucl. Instruments Methods Phys. Res. Sect. B Beam Interact. with Mater. Atoms*. (2010). doi:10.1016/j.nimb.2010.02.091.
- [20] M.K. Miller, K.F. Russell, K. Thompson, R. Alvis, D.J. Larson, Review of atom probe FIB-based specimen preparation methods, in: *Microsc. Microanal.*, 2007. doi:10.1017/S1431927607070845.
- [21] M.K. Miller, *Atom probe tomography : analysis at the atomic level*, Kluwer Academic/Plenum Publishers, New York ; London, 2000.
- [22] C.A. Williams, D. Haley, E.A. Marquis, G.D.W. Smith, M.P. Moody, Defining clusters in APT reconstructions of ODS steels, *Ultramicroscopy*. (2013). doi:10.1016/j.ultramic.2012.12.011.
- [23] M.K. Miller, R. Forbes, ProQuest (Firm), *Atom probe tomography : the local electrode atom probe*, (2014) 1 online resource (437 pages).
- [24] M.K. Miller, E.A. Kenik, *Atom probe tomography: A technique for nanoscale characterization*, in: *Microsc. Microanal.*, 2004. doi:10.1017/S1431927604040577.
- [25] R.S. Nelson, J.A. Hudson, D.J. Mazey, The stability of precipitates in an irradiation environment, *J. Nucl. Mater.* 44 (1972) 318–330. doi:10.1016/0022-3115(72)90043-8.
- [26] V. de Castro, T. Leguey, M.A. Auger, S. Lozano-Perez, M.L. Jenkins, Analytical characterization of secondary phases and void distributions in an ultrafine-grained ODS Fe–14Cr model alloy, *J. Nucl. Mater.* 417 (2011) 217–220. doi:10.1016/J.JNUCMAT.2010.12.067.
- [27] M.A. Auger, V. de Castro, T. Leguey, S. Lozano-Perez, P.A.J. Bagot, M.P. Moody, S.G. Roberts, Effect of the milling atmosphere on the microstructure and mechanical properties of a ODS Fe-14Cr model alloy, *Mater. Sci. Eng. A*. (2016). doi:10.1016/j.msea.2016.06.054.
- [28] D.A. Porter, K.E. Easterling, M.Y. Sherif, *Phase Transformations in Metals and Alloys*, Third Edition, 2009.
- [29] J. He, F. Wan, K. Sridharan, T.R. Allen, A. Certain, Y.Q. Wu, Response of 9Cr-ODS steel to proton irradiation at 400 °C, *J. Nucl. Mater.* (2014). doi:10.1016/j.jnucmat.2014.05.004.
- [30] J. He, F. Wan, K. Sridharan, T.R. Allen, A. Certain, V. Shutthanandan, Y.Q. Wu, Stability of nanoclusters in 14YWT oxide dispersion strengthened steel under heavy ion-

- irradiation by atom probe tomography, *J. Nucl. Mater.* (2014). doi:10.1016/j.jnucmat.2014.03.024.
- [31] M.J. Swenson, J.P. Wharry, The comparison of microstructure and nanocluster evolution in proton and neutron irradiated Fe-9%Cr ODS steel to 3 dpa at 500 °C, *J. Nucl. Mater.* (2015). doi:10.1016/j.jnucmat.2015.09.022.
 - [32] G.S. Was, J.P. Wharry, B. Frisbie, B.D. Wirth, D. Morgan, J.D. Tucker, T.R. Allen, Assessment of radiation-induced segregation mechanisms in austenitic and ferritic-martensitic alloys, *J. Nucl. Mater.* 411 (2011) 41–50. doi:10.1016/j.jnucmat.2011.01.031.
 - [33] Z. Jiao, G.S. Was, Segregation behavior in proton- and heavy-ion-irradiated ferritic-martensitic alloys, *Acta Mater.* (2011). doi:10.1016/j.actamat.2011.03.070.
 - [34] V. de Castro, S. Lozano-Perez, M. Briceno, P. Trocellier, S.G. Roberts, R. Pareja, Effects of single- and simultaneous triple-ion-beam irradiation on an oxide dispersion-strengthened Fe12Cr steel, *J. Mater. Sci.* (2015). doi:10.1007/s10853-014-8794-y.
 - [35] J.B. Seol, D. Haley, D.T. Hoelzer, J.H. Kim, Influences of interstitial and extrusion temperature on grain boundary segregation, Y–Ti–O nanofeatures, and mechanical properties of ferritic steels, *Acta Mater.* 153 (2018) 71–85. doi:10.1016/J.ACTAMAT.2018.04.046.
 - [36] T.R. Allen, J. Gan, J.I. Cole, M.K. Miller, J.T. Busby, S. Shutthanandan, S. Thevuthasan, Radiation response of a 9 chromium oxide dispersion strengthened steel to heavy ion irradiation, *J. Nucl. Mater.* (2008). doi:10.1016/j.jnucmat.2007.11.001.
 - [37] S. Choudhury, L. Barnard, J.D. Tucker, T.R. Allen, B.D. Wirth, M. Asta, D. Morgan, Ab-initio based modeling of diffusion in dilute bcc Fe–Ni and Fe–Cr alloys and implications for radiation induced segregation, *J. Nucl. Mater.* (2011). doi:10.1016/j.jnucmat.2010.12.231.
 - [38] T.R. Allen, D. Kaoumi, J.P. Wharry, Z. Jiao, C. Topbasi, A. Kohnert, L. Barnard, A. Certain, K.G. Field, G.S. Was, D.L. Morgan, A.T. Motta, B.D. Wirth, Y. Yang, Characterization of microstructure and property evolution in advanced cladding and duct: Materials exposed to high dose and elevated temperature, *J. Mater. Res.* (2015). doi:10.1557/jmr.2015.99.
 - [39] A.J. Arderl, *Materials Issues for Generation IV Systems*, 2008. doi:10.1007/978-1-4020-8422-5.
 - [40] R. Hu, G.D.W. Smith, E.A. Marquis, Atom probe study of radiation induced grain boundary segregation/depletion in a Fe-12%Cr alloy, in: *Prog. Nucl. Energy*, Pergamon, 2012: pp. 14–19. doi:10.1016/j.pnucene.2011.10.011.
 - [41] C. Zheng, J.-H. Ke, S.A. Maloy, D. Kaoumi, Correlation of in-situ transmission electron microscopy and microchemistry analysis of radiation-induced precipitation and segregation in ion irradiated advanced ferritic/martensitic steels, *Scr. Mater.* 162 (2019) 460–464. doi:https://doi.org/10.1016/j.scriptamat.2018.12.018.

- [42] G.S. Was, S. Taller, Z. Jiao, A.M. Monterrosa, D. Woodley, D. Jennings, T. Kubley, F. Naab, O. Toader, E. Uberseder, Resolution of the carbon contamination problem in ion irradiation experiments, Nucl. Instruments Methods Phys. Res. Sect. B Beam Interact. with Mater. Atoms. (2017). doi:10.1016/j.nimb.2017.08.039.
- [43] D.T. Hoelzer, K.A. Unocic, M.A. Sokolov, T.S. Byun, Influence of processing on the microstructure and mechanical properties of 14YWT, J. Nucl. Mater. (2016). doi:10.1016/j.jnucmat.2015.12.011.

Figure legends

Fig. 1. (a) Extruded bars containing consolidated 14YWT. (b) Cross-rolled plate enclosed in mild steel can. (c) De-canned cross-rolled plate.

Fig. 2. 3D ion maps of as-received 14YWT showing (a) volume inside a grain and (b) volume containing grain boundaries.

Fig. 3. 3D ion maps of ion irradiated 14YWT showing a) volume inside a grain and b) volume containing grain boundaries.

Fig. 4. Size (Guinier diameter) distribution of clusters (a) inside grains and (b) at grain boundaries in as-received 14YWT and (c) inside grains and (d) in or close to grain boundaries in ion irradiated 14YWT.

Fig. 5. Chemistry of the clusters inside grains for 14YWT (a) as-received and (b) ion irradiated and in or close to grain boundaries for 14YWT (c) as-received and (d) ion irradiated.

Fig. 6. 1D chemical analysis through one grain boundary in as-received 14YWT.

Fig. 7. 1D chemical analysis through one grain boundary in irradiated 14YWT.

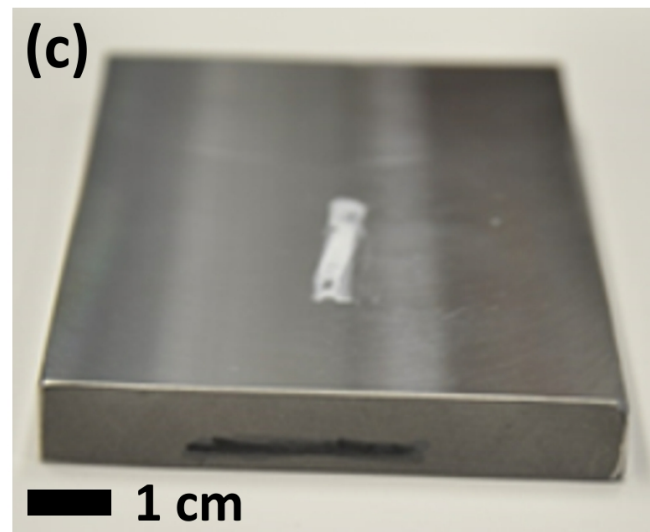
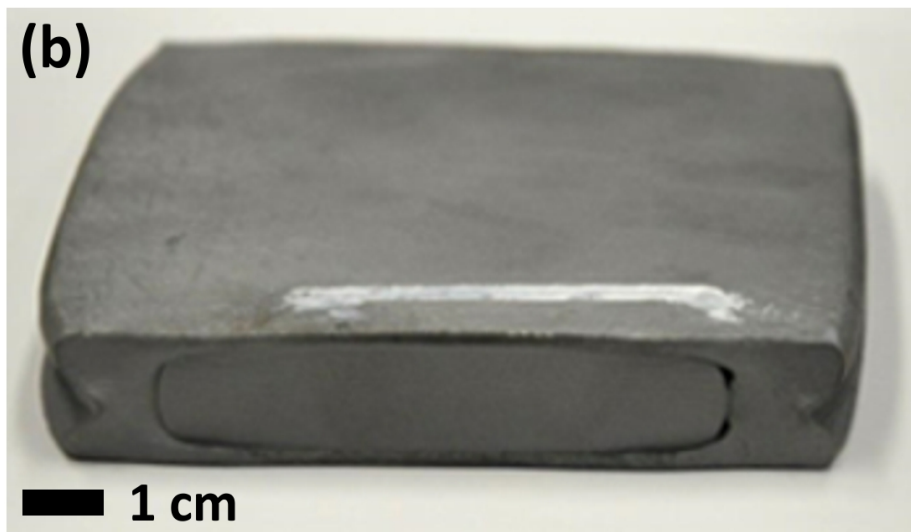
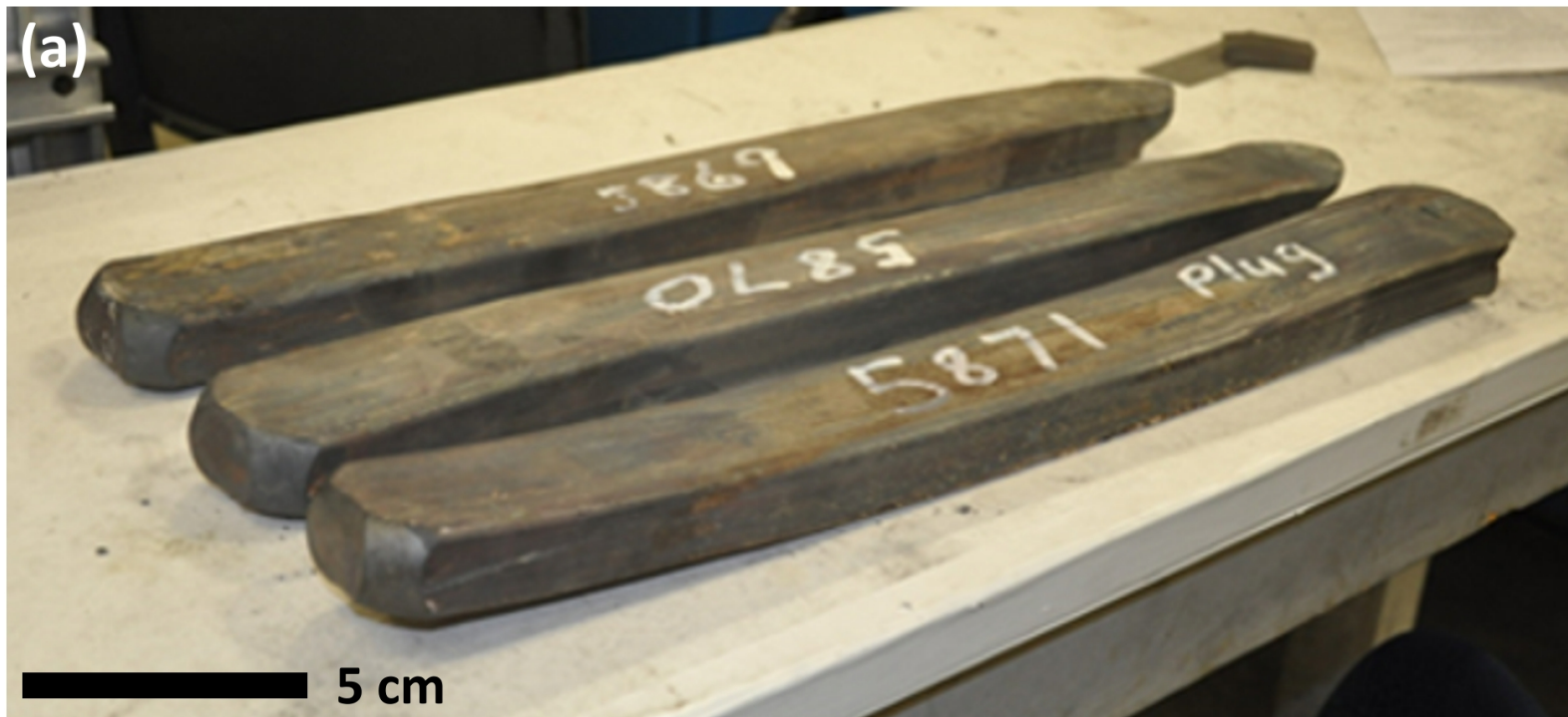
Additional data

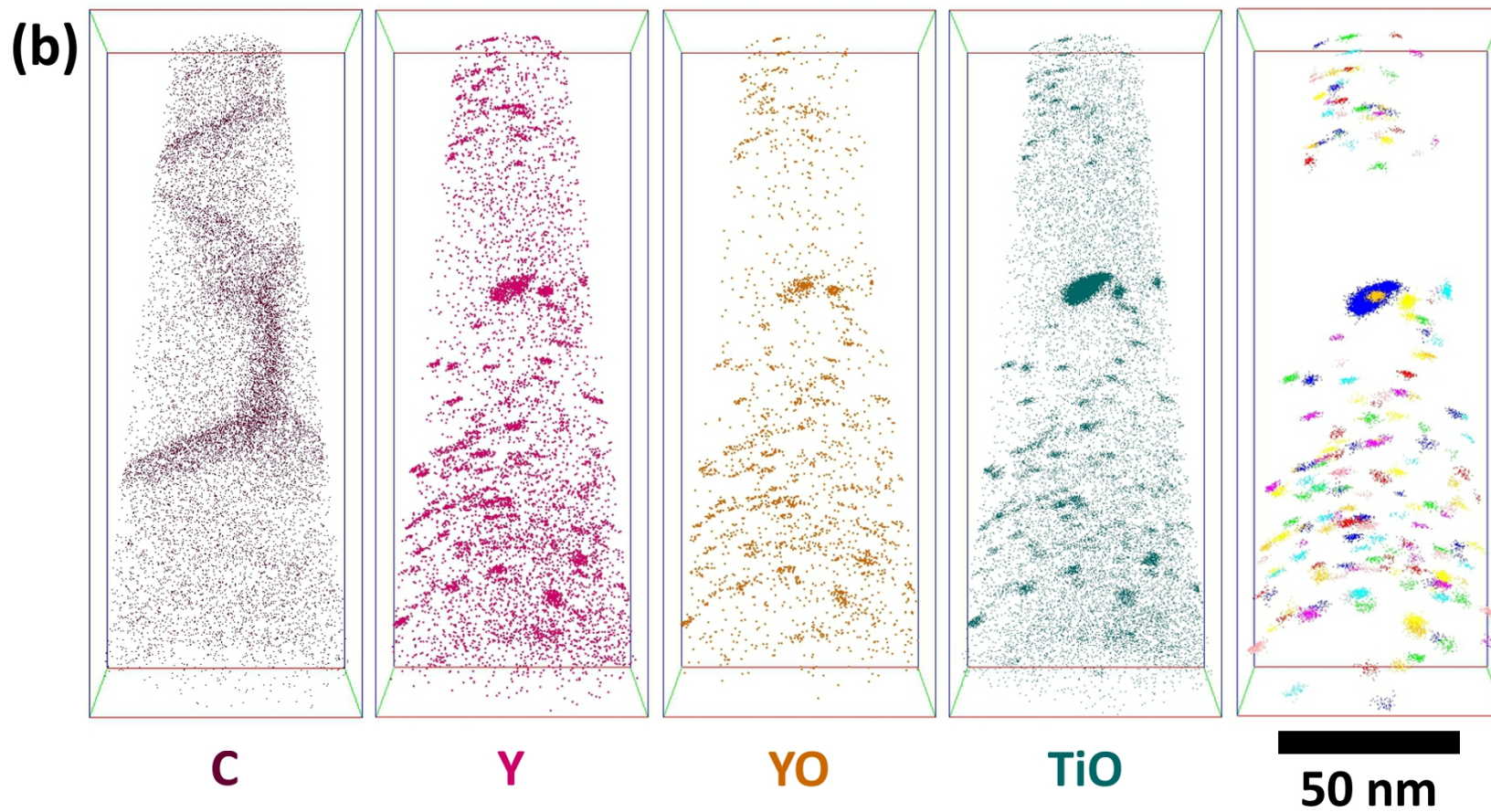
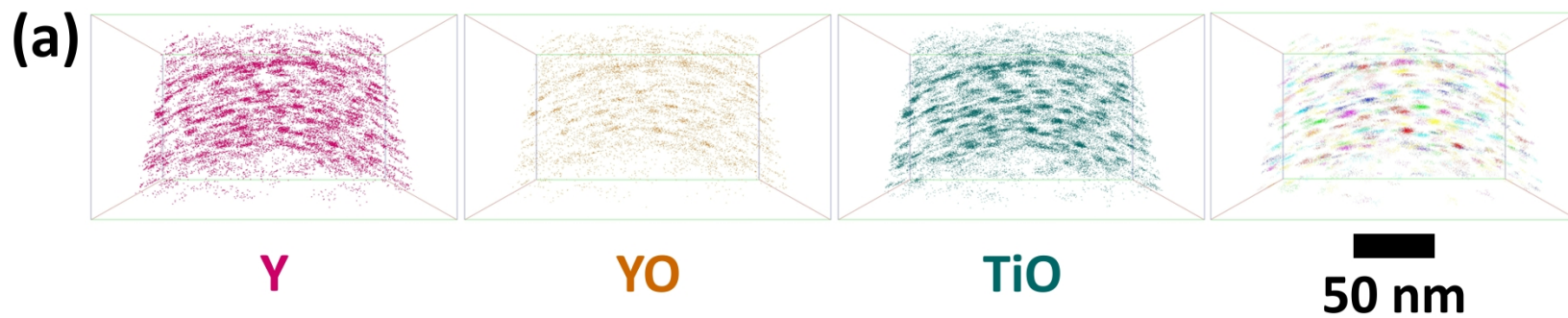
Fig. 8. Additional datasets of volumes inside grains in as-received 14YWT.

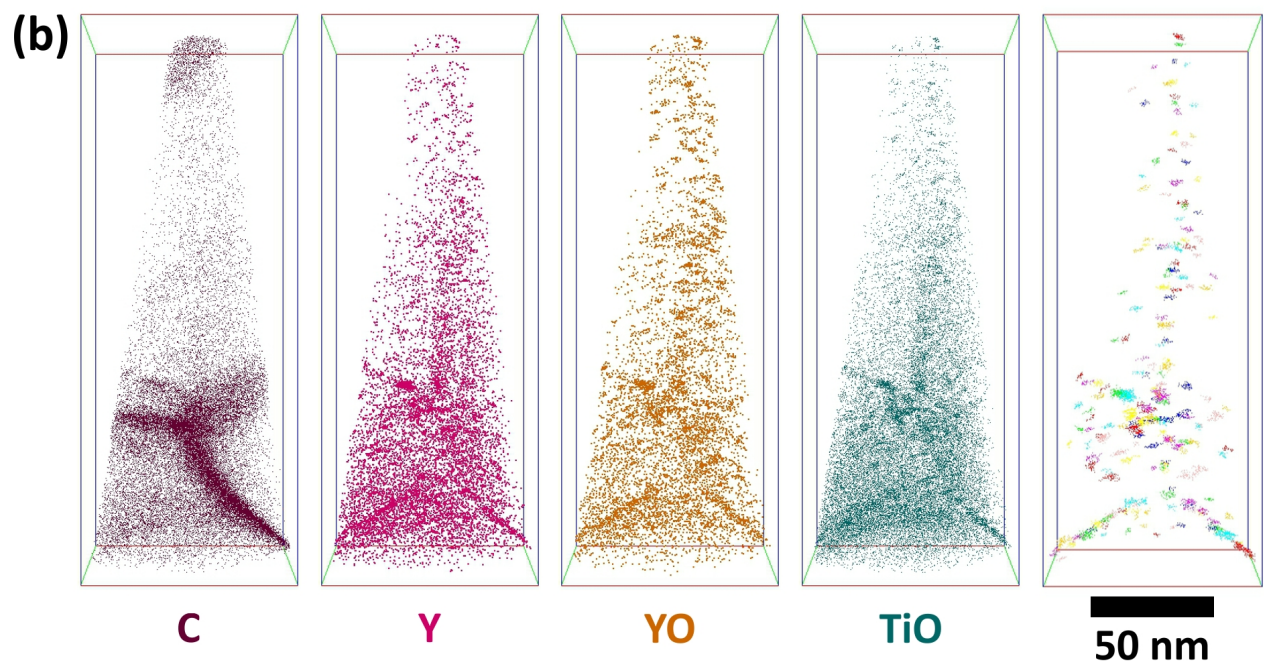
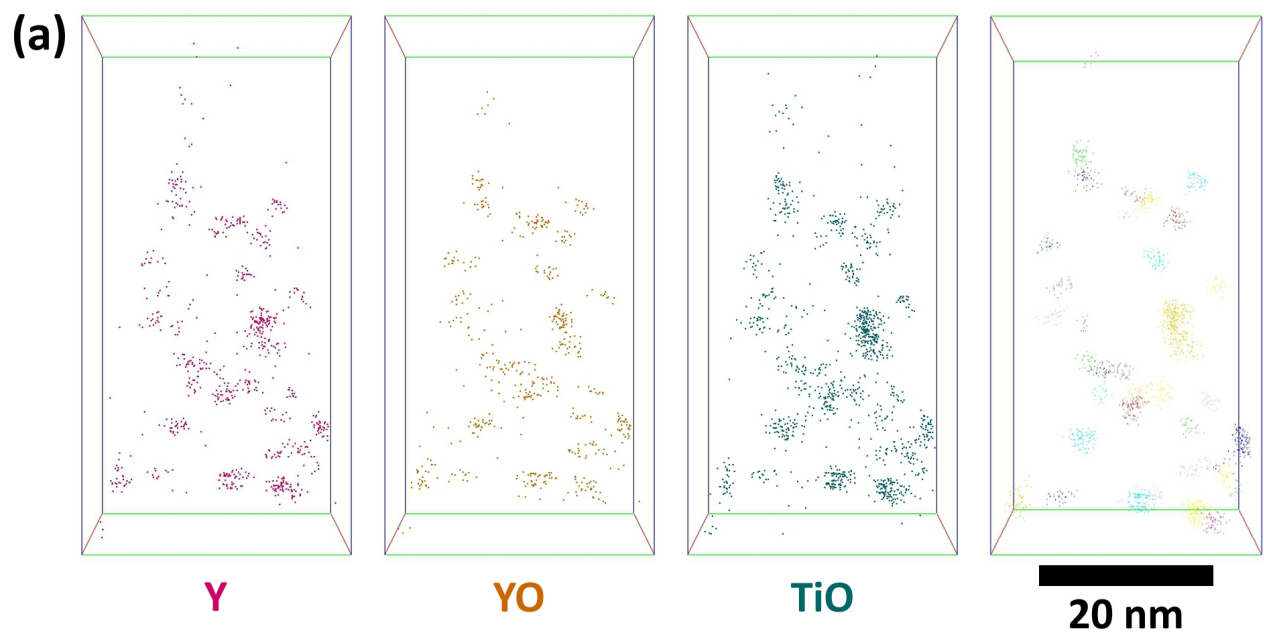
Fig. 9. Additional datasets of volumes containing grain boundaries in as-received 14YWT.

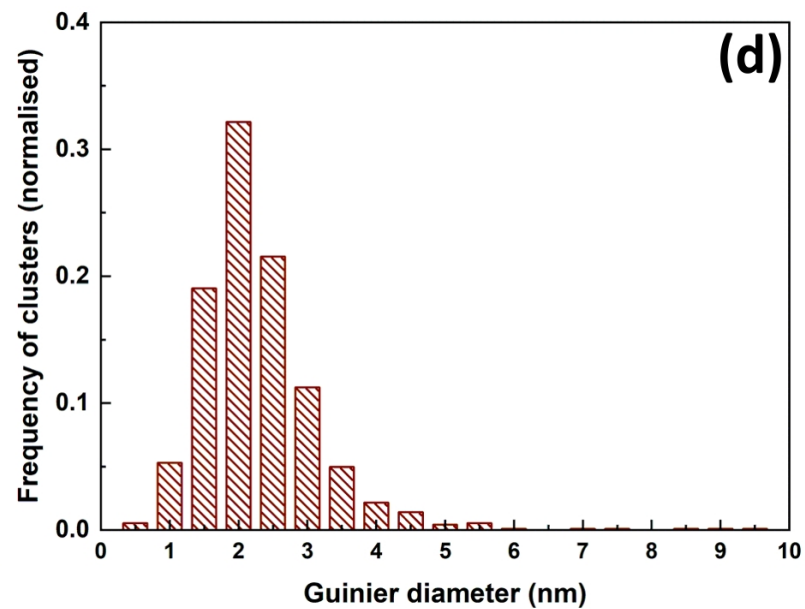
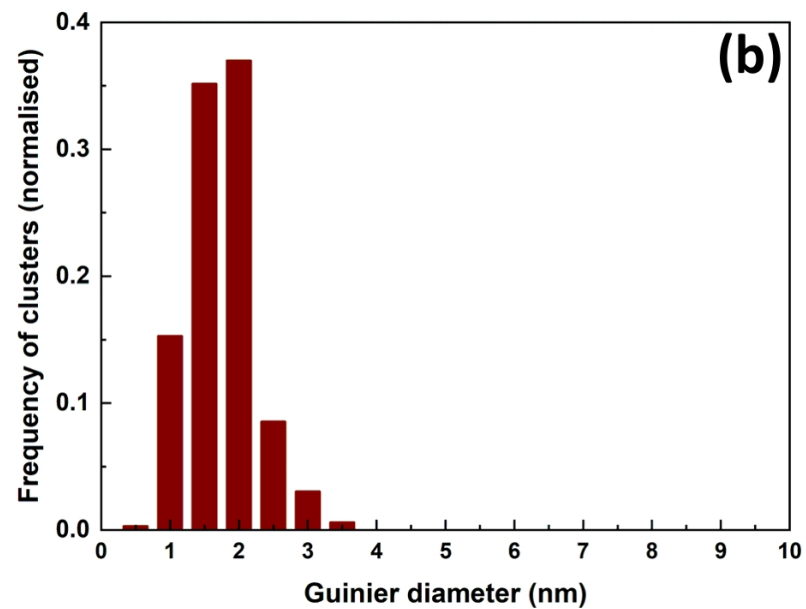
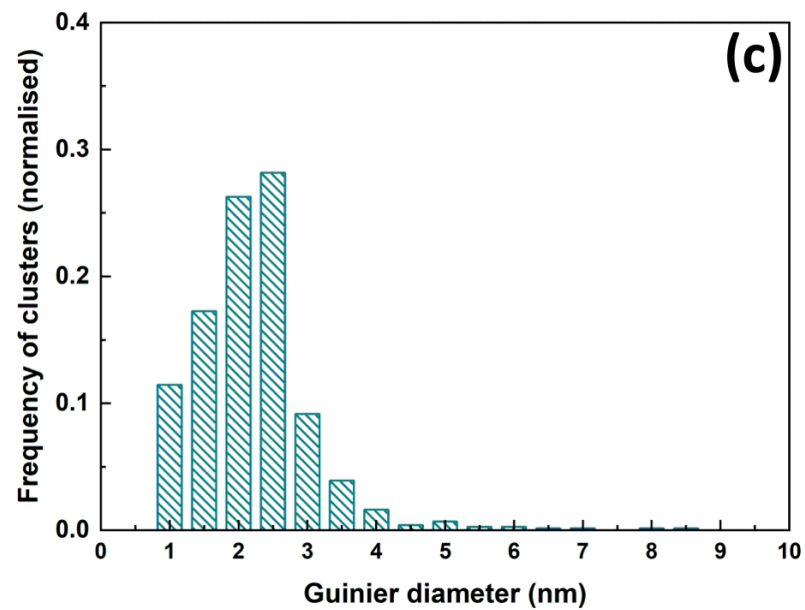
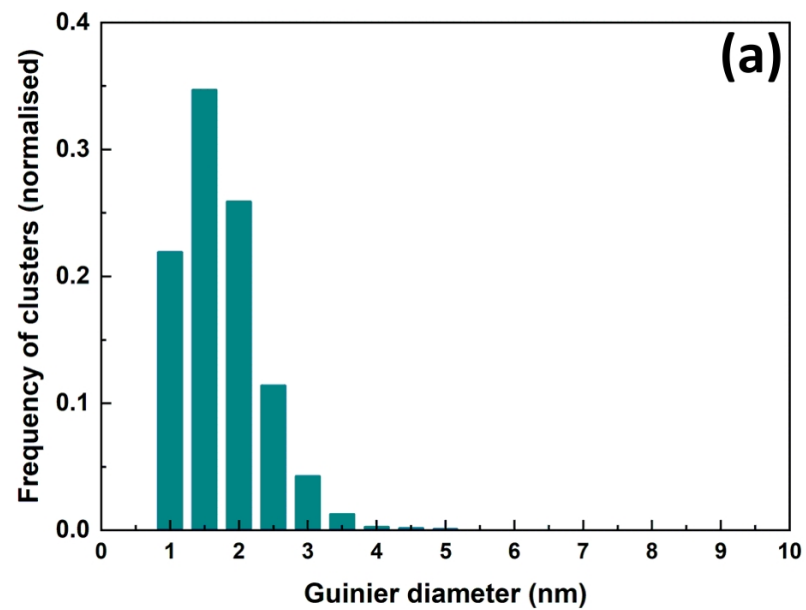
Fig. 10. Additional datasets of volumes inside grains in irradiated 14YWT.

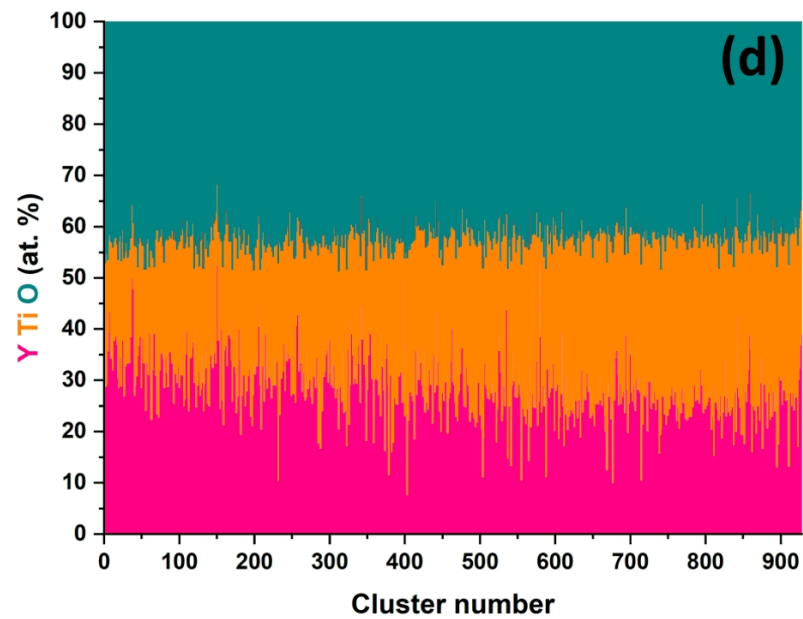
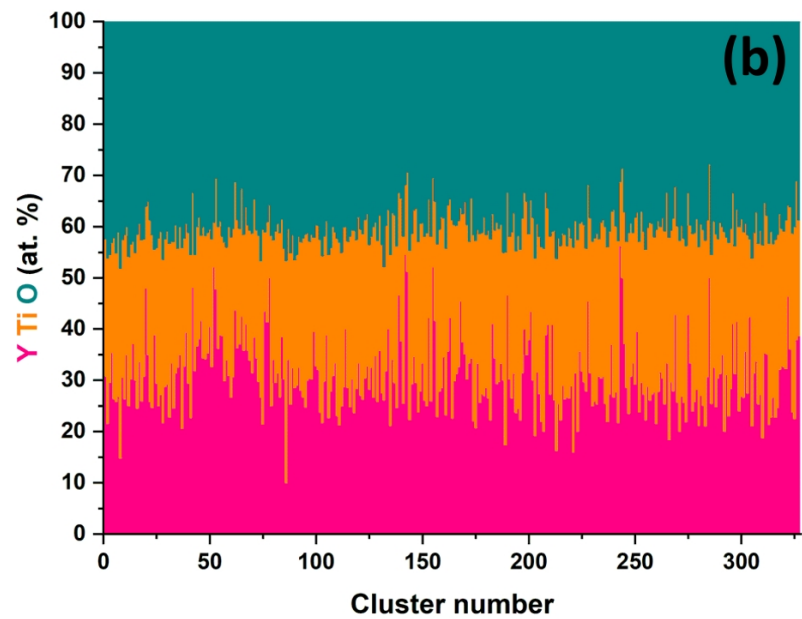
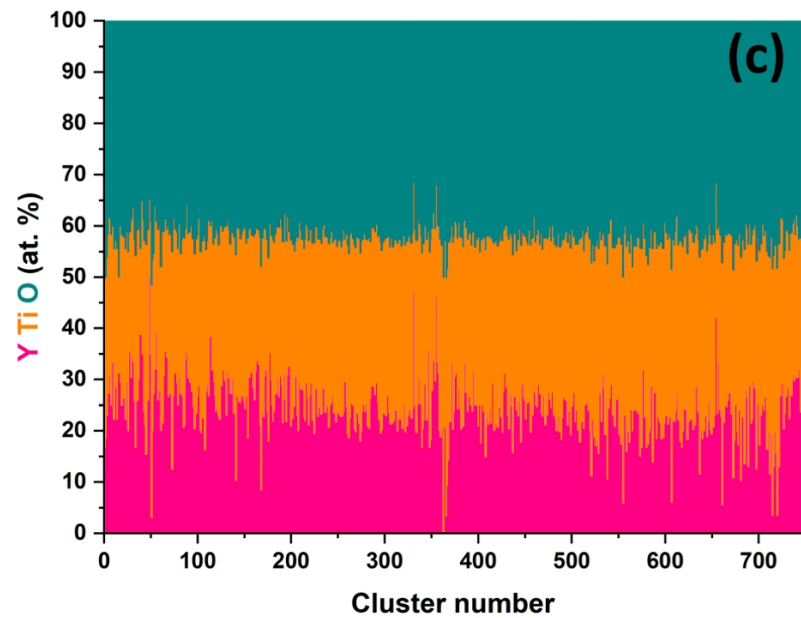
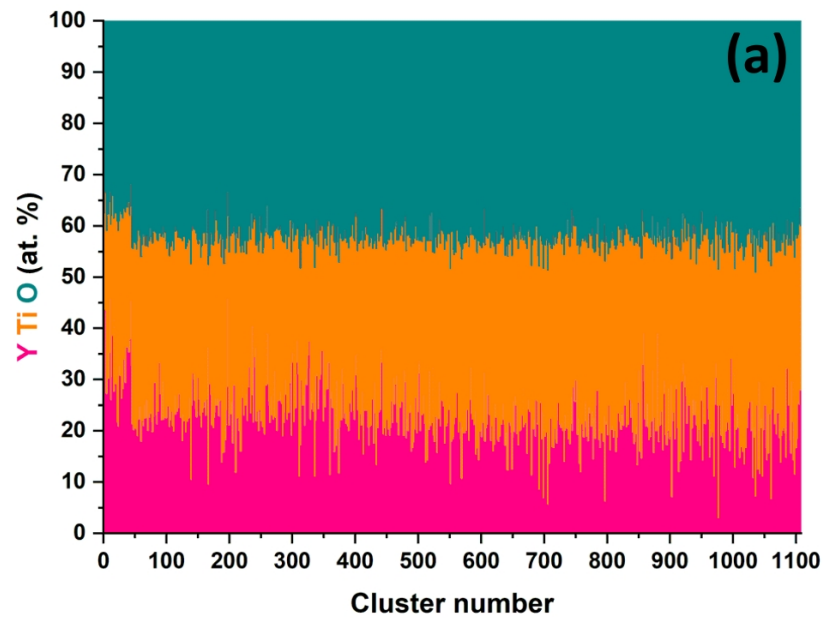
Fig. 11. Additional datasets of volumes containing grain boundaries in irradiated 14YWT.

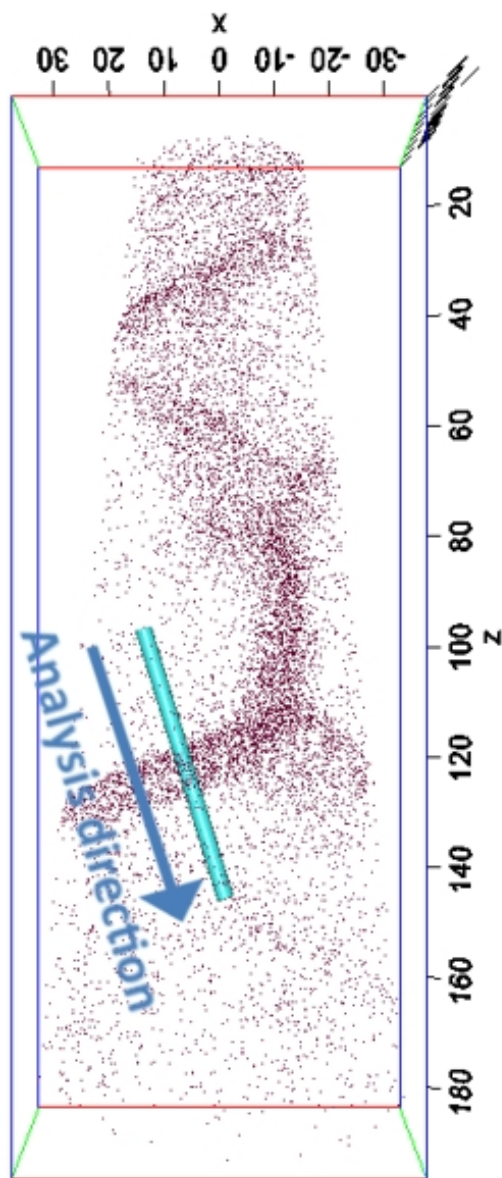




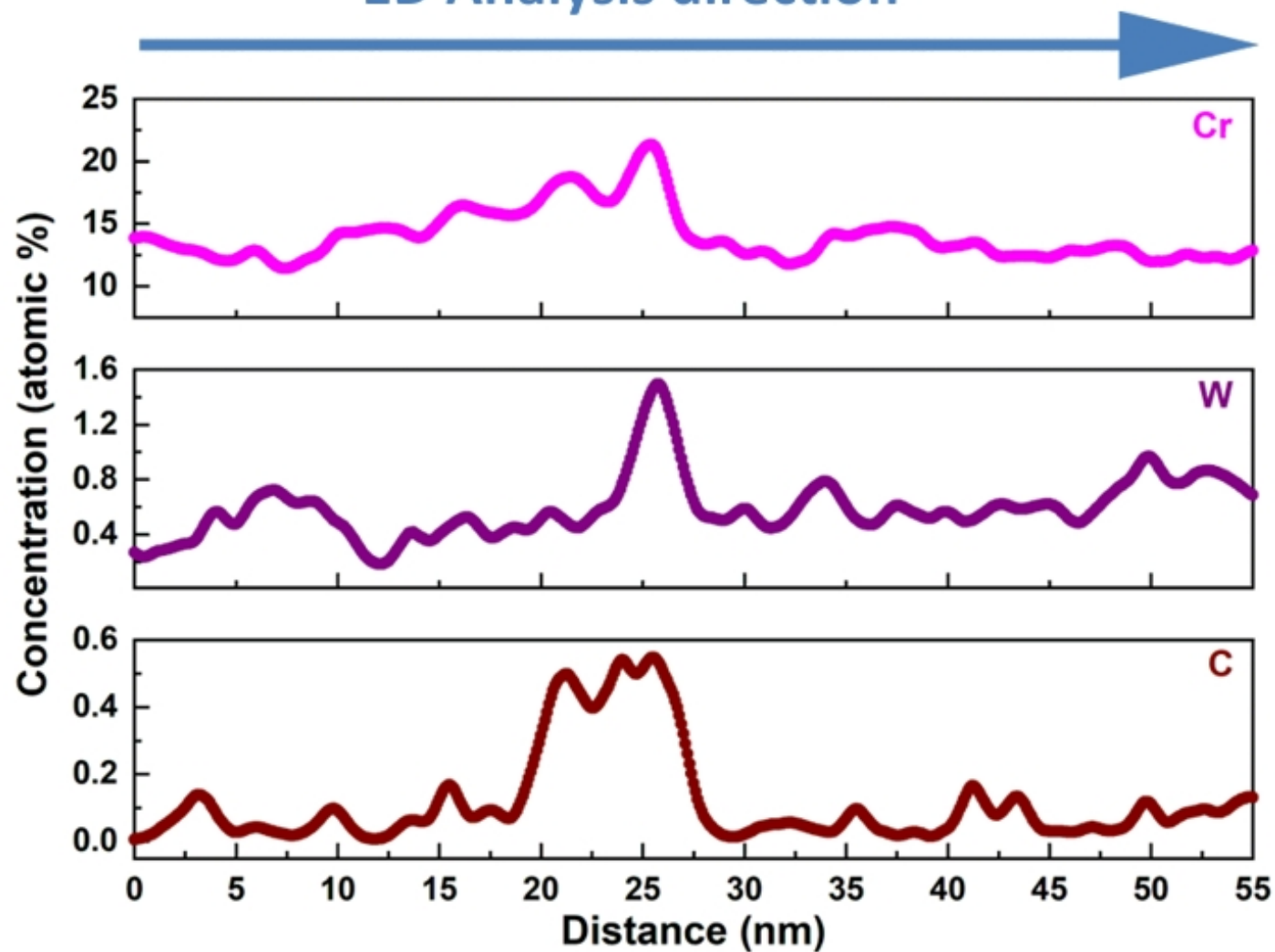


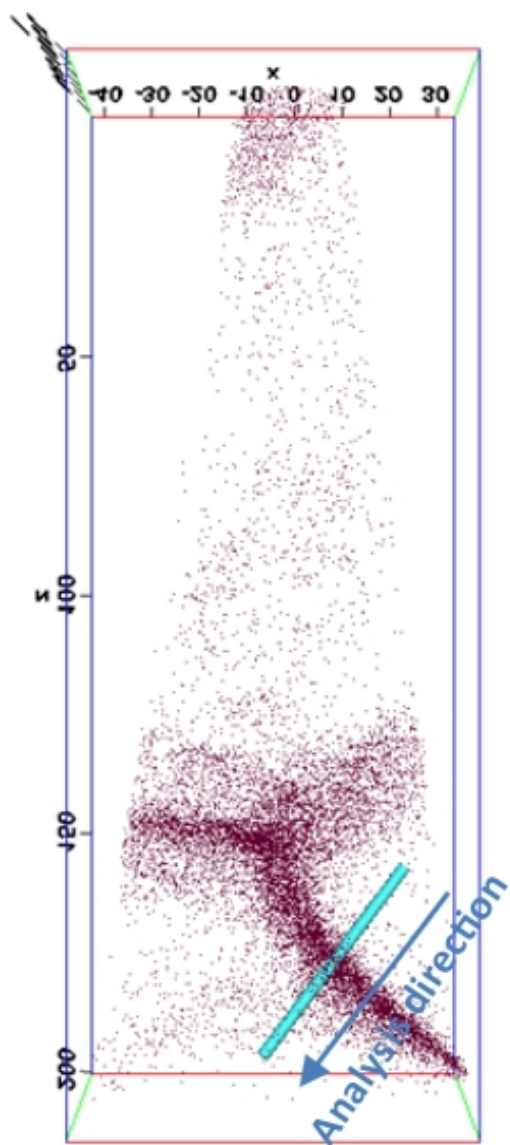




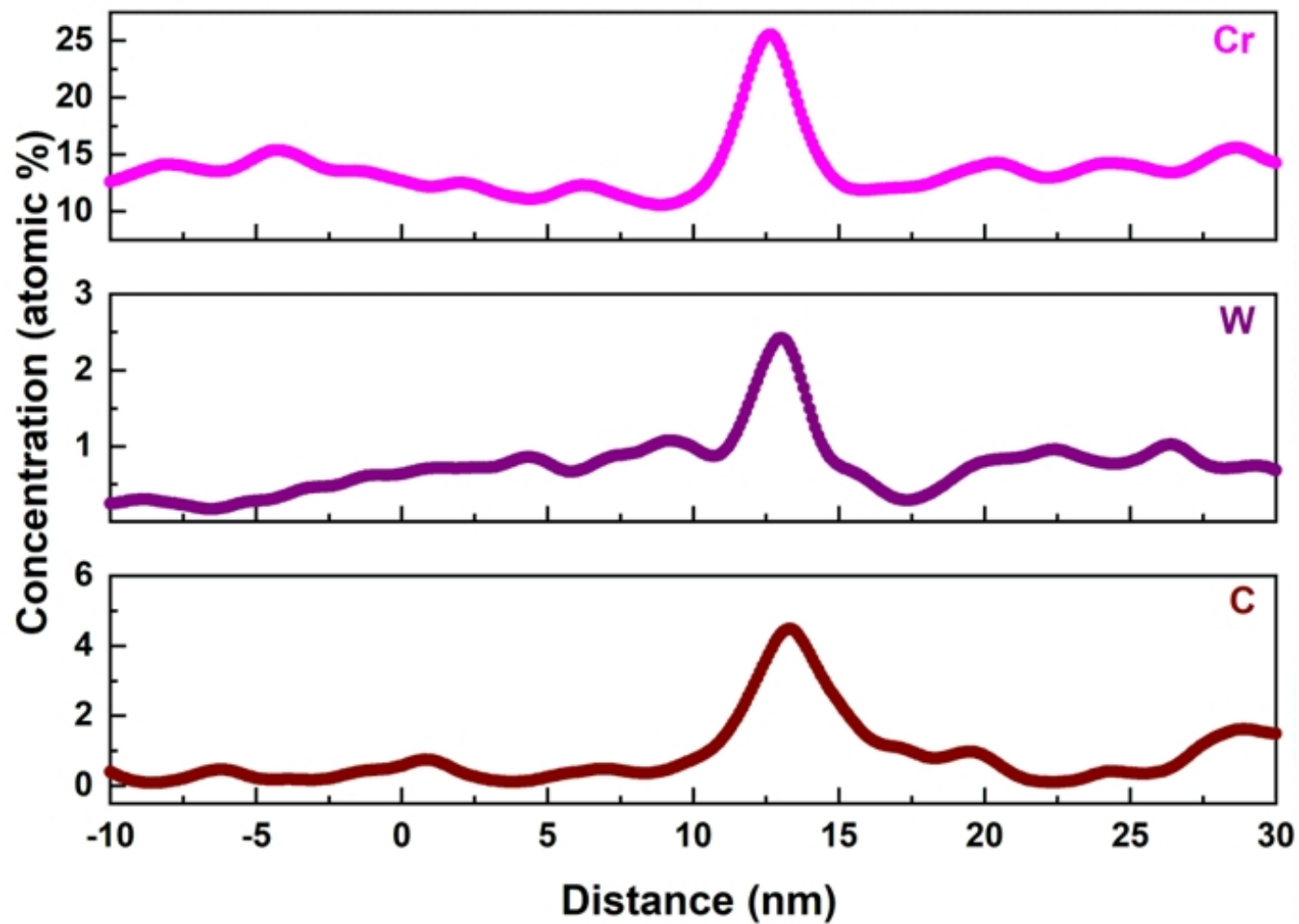


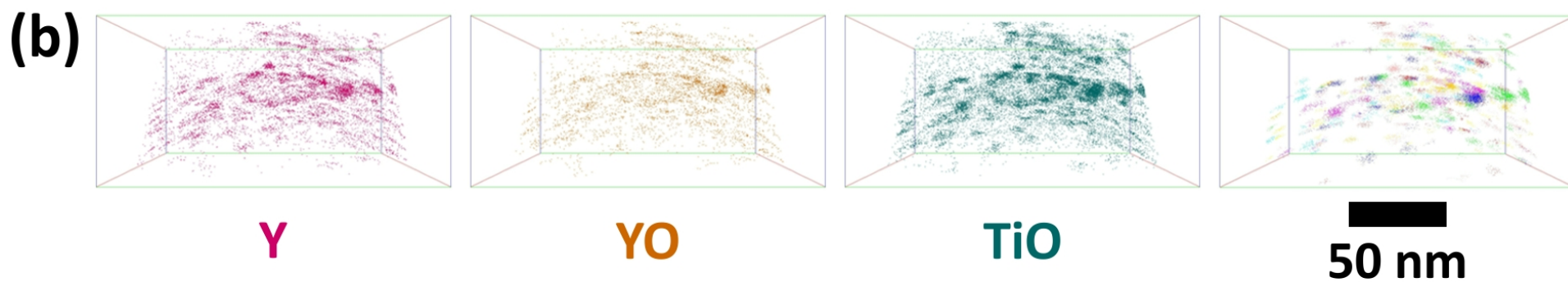
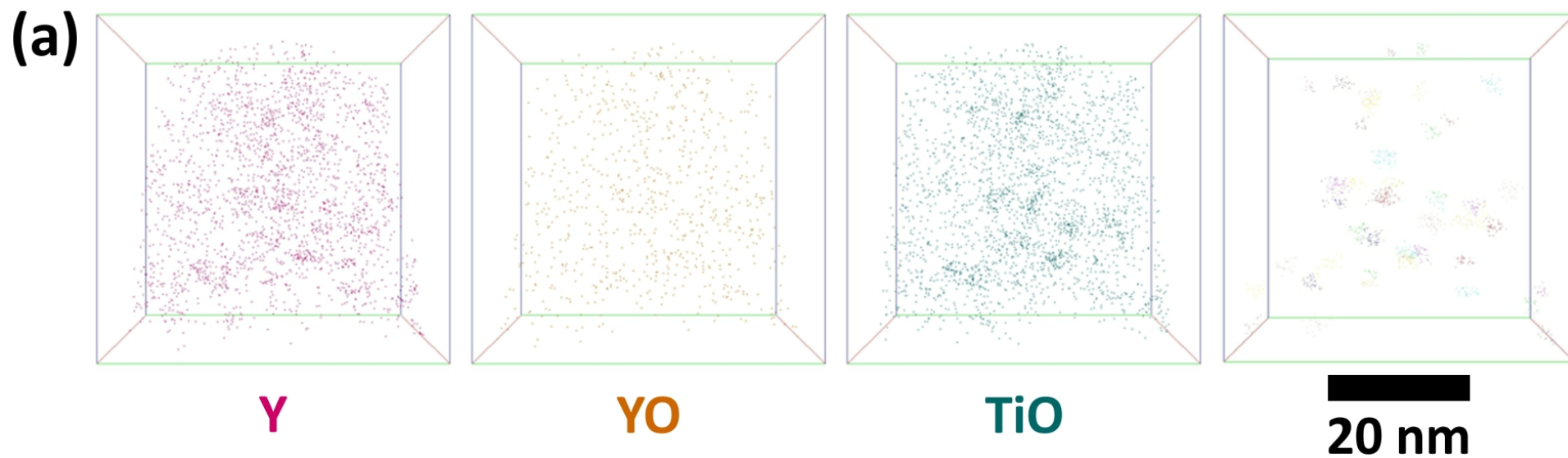
1D Analysis direction

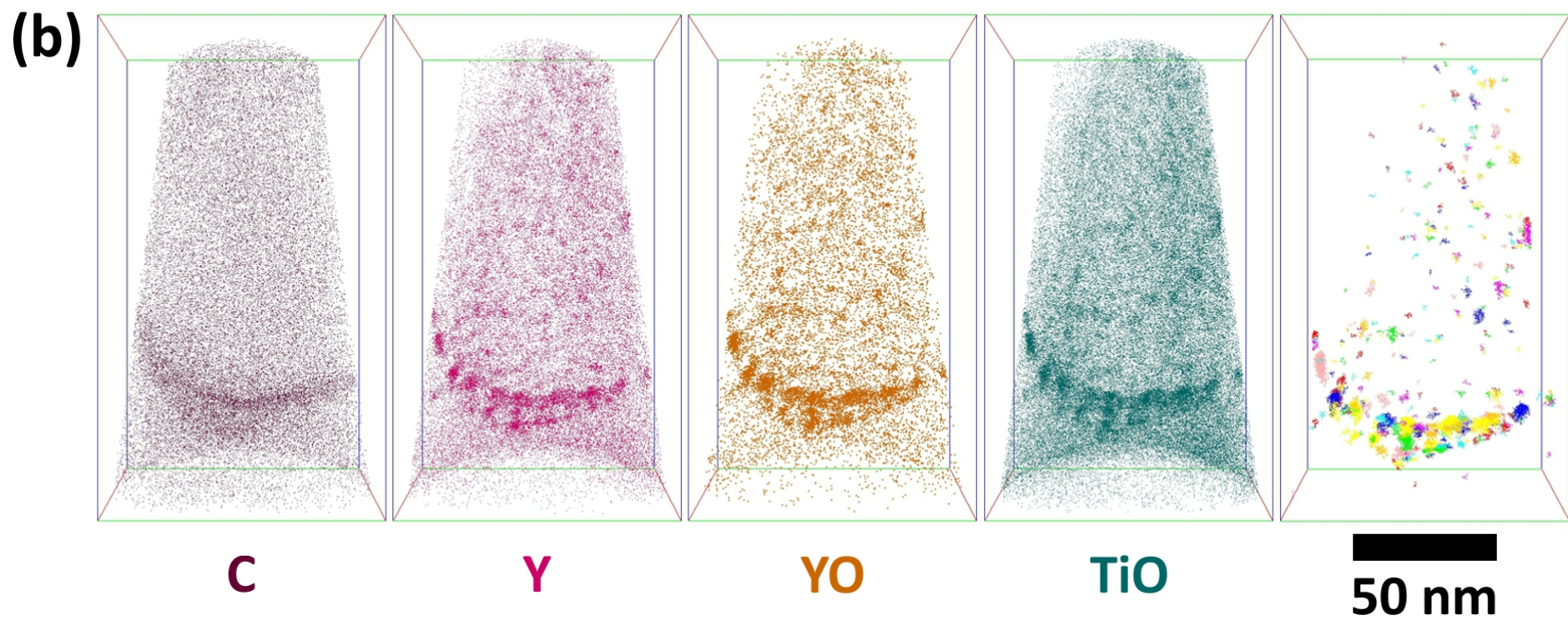
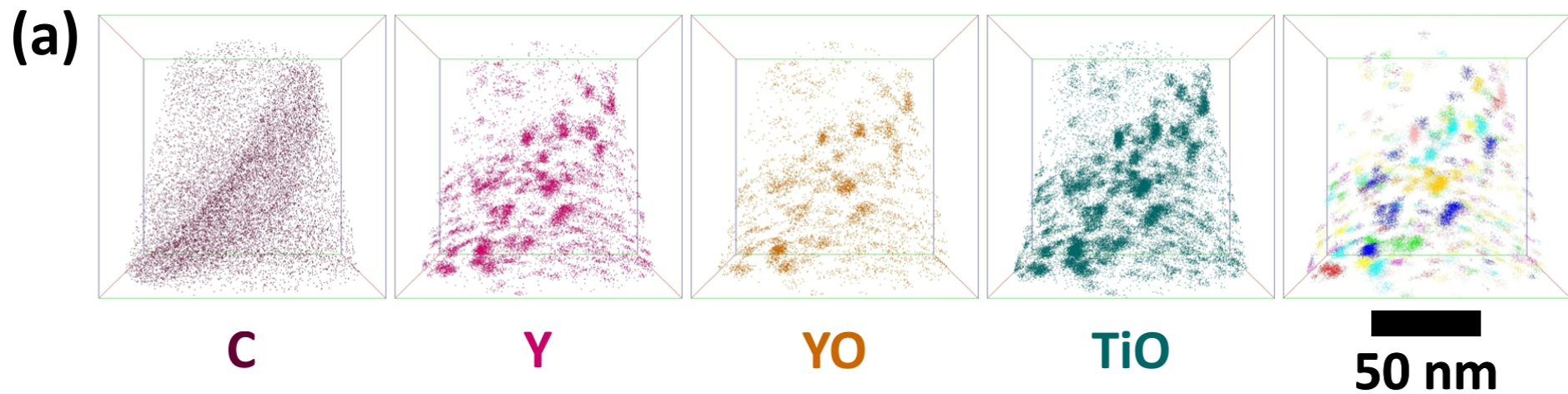


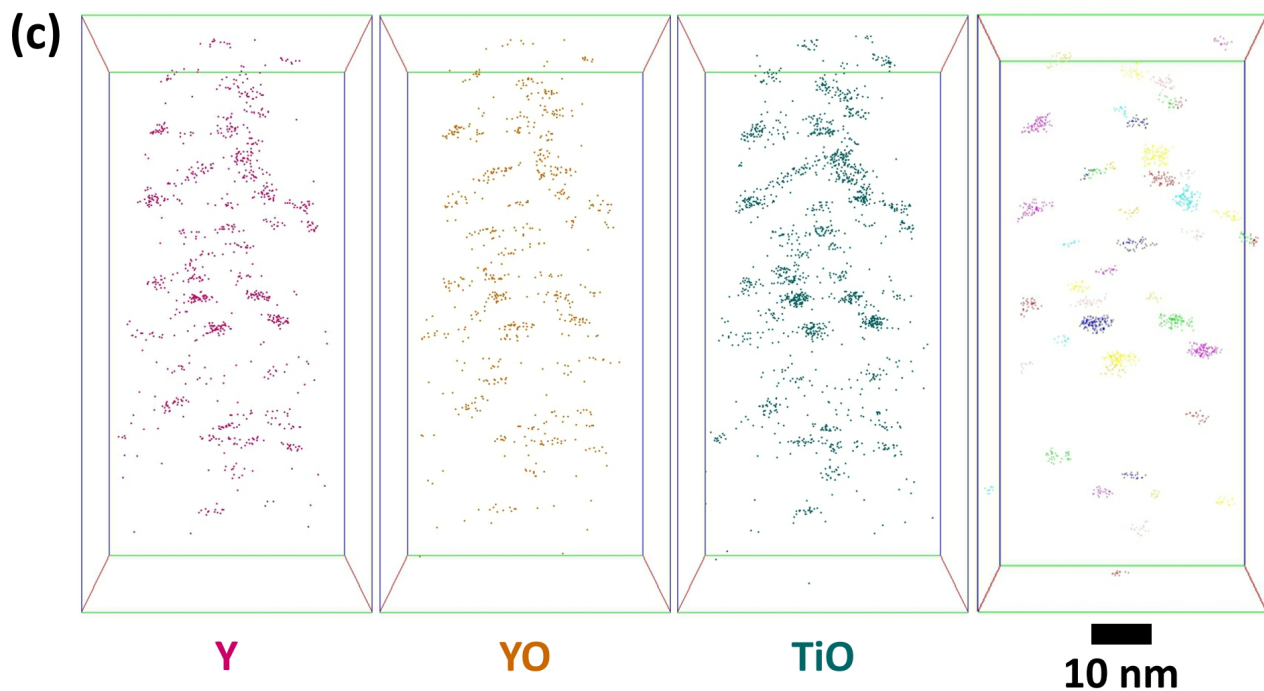
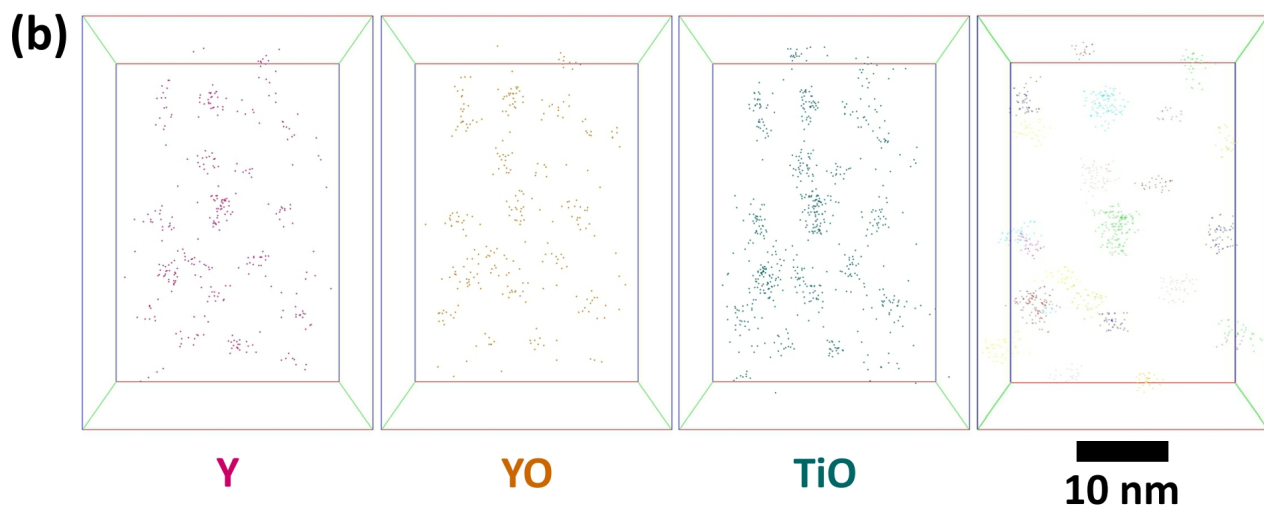
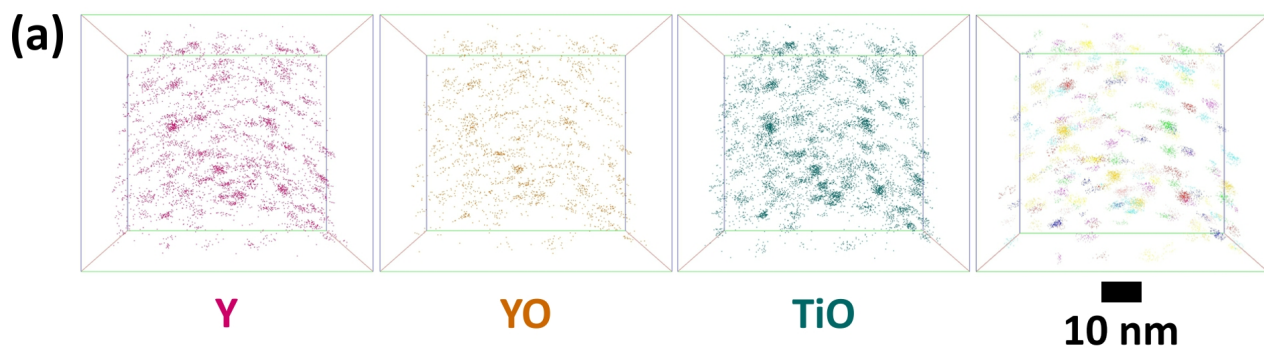


1D Analysis direction









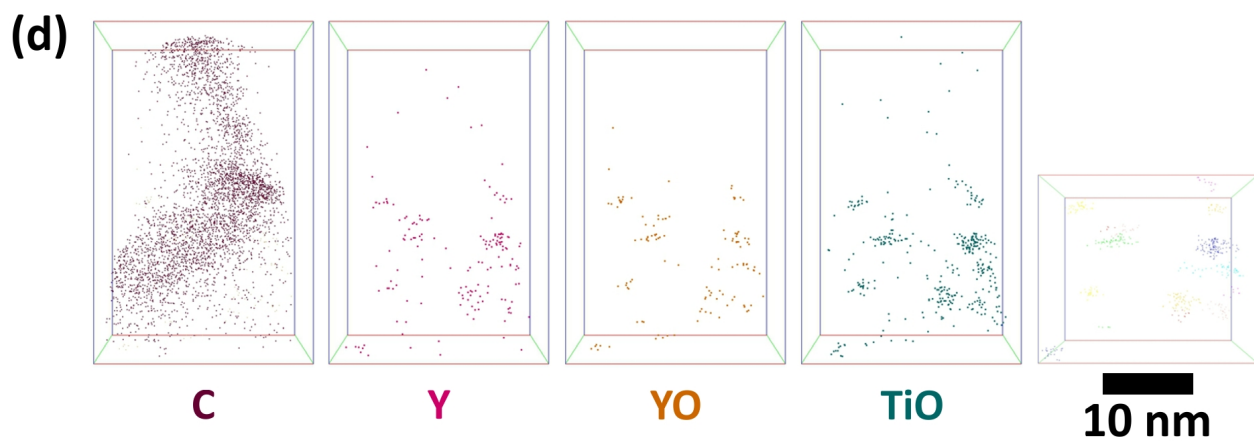
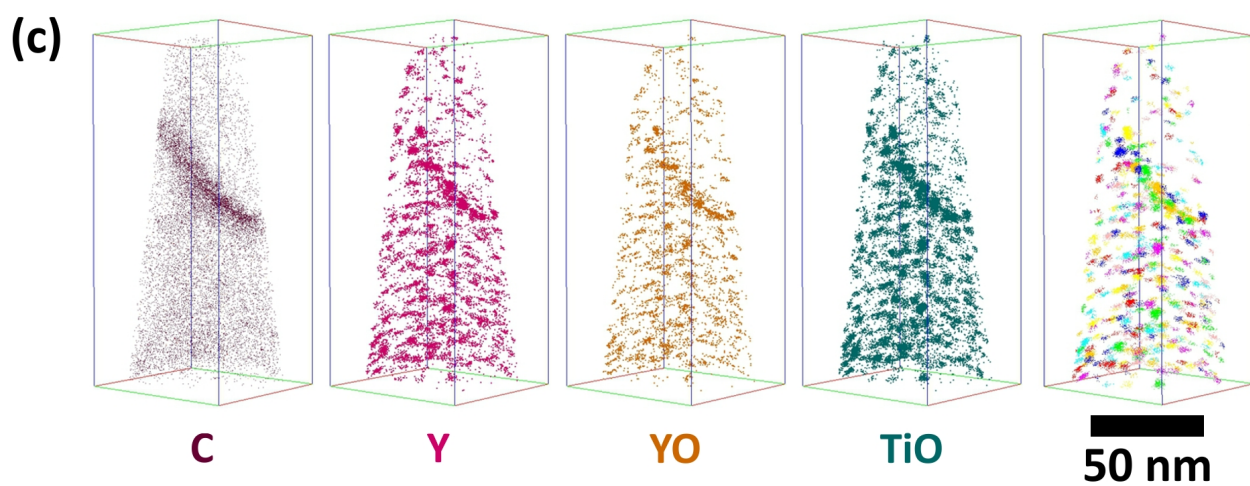
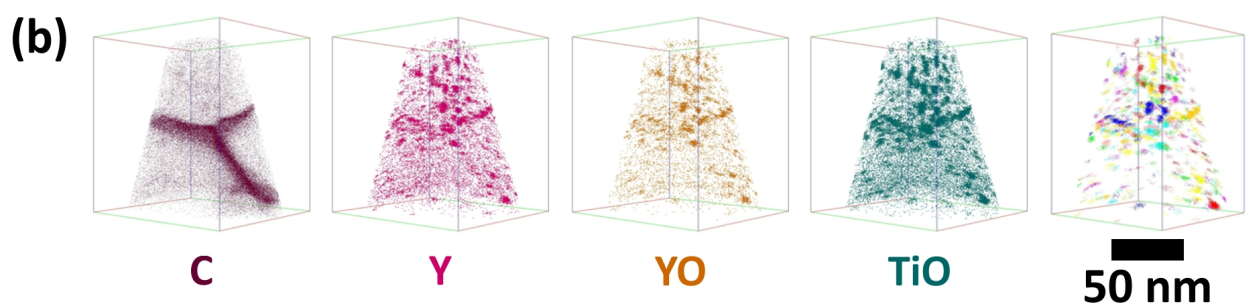
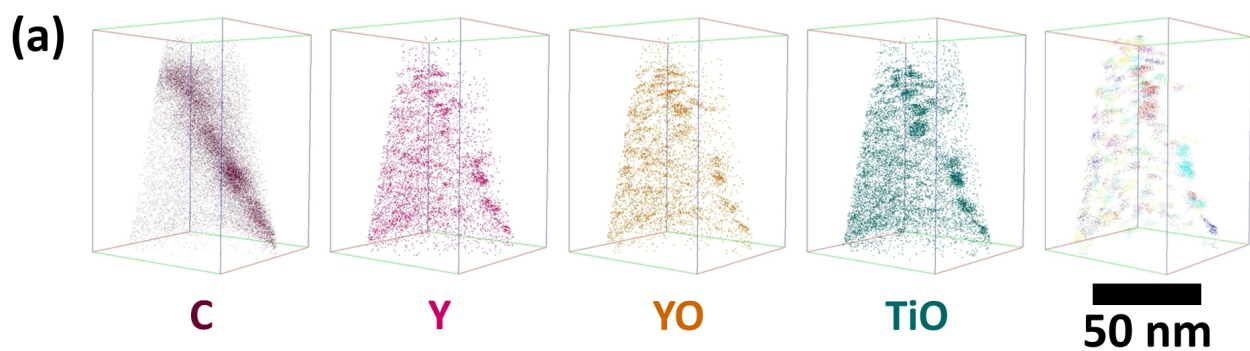


Table I. Bulk composition of as-received 14YWT (provided by ORNL) and APT results of bulk and matrix composition of as-received and ion irradiated 14YWT (at. %)

	Alloy Chemistry				
	ORNL results	14YWT as-received		14YWT irradiated	
	Bulk	Bulk	Matrix	Bulk	Matrix
Element	At. %	At. %	At. %	At. %	At. %
Fe	82.206	82.97 ± 0.72	83.13 ± 0.76	83.24 ± 1.12	83.47 ± 0.76
Cr	15.313	15.02 ± 0.42	15.05 ± 0.42	14.74 ± 0.31	15.15 ± 0.54
W	0.703	0.71 ± 0.18	0.75 ± 0.17	0.58 ± 0.24	0.52 ± 0.23
Ti	0.314	0.22 ± 0.10	0.14 ± 0.13	0.16 ± 0.06	0.06 ± 0.01
Y	0.119	0.12 ± 0.04	0.07 ± 0.05	0.11 ± 0.04	0.04 ± 0.04
O	0.616	0.46 ± 0.15	0.36 ± 0.18	0.51 ± 0.34	0.25 ± 0.15
N	0.394	0.17 ± 0.12	0.17 ± 0.12	0.15 ± 0.08	0.16 ± 0.06
C	0.111	0.15 ± 0.07	0.14 ± 0.07	0.42 ± 0.38	0.32 ± 0.37
Al	0.033	0.02 ± 0.02	0.02 ± 0.02	0.007 ± 0.006	0.006 ± 0.003
Si	0.085	0.08 ± 0.01	0.08 ± 0.02	0.05 ± 0.04	0.02 ± 0.02
P	0.016	0.005 ± 0.002	0.005 ± 0.002	0.003 ± 0.002	0.003 ± 0.002
Mn	0.008	0.02 ± 0.01	0.02 ± 0.01	0.02 ± 0.01	0.02 ± 0.01
Cu	0.030	0.04 ± 0.01	0.02 ± 0.02	0.001 ± 0.001	0.003 ± 0.003
Ni	0.011	0.018 ± 0.006	0.02 ± 0.01	0.007 ± 0.007	0.007 ± 0.007
S	0.005	----	----	----	----
Nb	0.001	----	----	----	----
Mo	0.000	----	----	----	----
Co	0.035	----	----	----	----

Table II. Summary of the cluster analysis statistics.

	Clusters inside grains		Clusters in or close to grain boundaries	
	14YWT as-received	14YWT irradiated	14YWT as-received	14YWT irradiated
Number of clusters	1104	327	742	924
Cluster size range (nm)	0.76 - 4.85	0.62 - 3.60	0.82 - 8.37	0.37 -9.34
Median cluster size (nm)	1.64	1.74	2.19	2.13
Average cluster size (nm)	1.74 ± 0.59	1.75 ± 0.49	2.21 ± 0.86	2.29 ± 0.90
Number density of clusters ($\times 10^{24} \text{ m}^{-3}$)	1.49 ± 0.25	2.08 ± 0.71	0.94 ± 0.69	1.37 ± 0.87
Distance between nearest neighbor clusters (nm)	6.82 ± 2.60	6.52 ± 2.19	7.24 ± 3.10	7.02 ± 2.25

Table III. Summary of the cluster composition.

	Clusters inside grains		Clusters in or close to grain boundaries	
	14YWT as-received	14YWT irradiated	14YWT as-received	14YWT irradiated
Y (at. %)	26.83 ± 8.36	30.66 ± 7.29	27.01 ± 8.07	31.78 ± 8.38
Ti (at. %)	32.75 ± 5.49	28.95 ± 5.30	31.94 ± 5.63	27.35 ± 6.69
O (at. %)	40.42 ± 3.74	40.39 ± 3.44	41.04 ± 3.29	40.87 ± 3.50
Y:Ti	0.91 ± 0.69	1.16 ± 0.62	0.94 ± 0.74	1.38 ± 1.10
(Y+Ti):O	1.50 ± 0.31	1.50 ± 0.24	1.45 ± 0.23	1.47 ± 0.26

Table IV. Summary of peak composition and interface width at the grain boundaries.

	14YWT as-received	14YWT irradiated
C (at. %)	0.47 ± 0.15	3.97 ± 1.58
W (at. %)	1.20 ± 0.43	1.31 ± 0.64
Cr (at. %)	19.91 ± 1.48	25.37 ± 4.13
Interface width (nm)	11.02 ± 3.60	8.80 ± 2.00
Number of analyzed interfaces	5	10

Conflict of Interest and Authorship Conformation Form

Please check the following as appropriate:

- ✓ All authors have participated in (a) conception and design, or analysis and interpretation of the data; (b) drafting the article or revising it critically for important intellectual content; and (c) approval of the final version.
- ✓ This manuscript has not been submitted to, nor is under review at, another journal or other publishing venue.
- ✓ The authors have no affiliation with any organization with a direct or indirect financial interest in the subject matter discussed in the manuscript
- ✗ The following authors have affiliations with organizations with direct or indirect financial interest in the subject matter discussed in the manuscript:

Author's name

Affiliation

[illegible]